

Theory of transport property of density wave phases in three-dimensional metals and semimetals under high magnetic field

Xiao-Tian Zhang^{1,2} and Ryuichi Shindou^{1,2,*}

¹*International Center for Quantum Materials, Beijing, 100871, China*

²*Collaborative Innovation Center of Quantum Matter, Beijing, 100871, China*

Three-dimensional (3D) metals/semimetals under magnetic field have an instability toward a density wave (DW) ordering which breaks a translational symmetry along the field direction. Effective boson models for the DW phases take forms of XY models with/without Potts terms. Longitudinal conductivity along the field direction is calculated in the DW phases with inclusion of effects of low-energy charge fluctuation (phason) and disorder. A single-particle imaginary-time Green function is identified with a partition function of 3D XY models in the presence of pairs of magnetic monopoles. In terms of the celebrated electromagnetic duality, electronic spectral function is calculated near the DW phase transition. The calculated result shows that the single-particle spectral function acquires an additional low-energy feature due to the strong phason fluctuation. Relevance to an in-plane conductance due to surface chiral Fermi arc states are also discussed.

PACS numbers:

I. INTRODUCTION

An investigation of magnetic-field-induced many-body states in three dimensional (3D) metal and semimetal has a distinguished history¹. Unlike the two-dimensional case, where the kinetic energy is completely quenched, the 3D metal/semimetal under high magnetic field has one-dimensional electronic dispersions along the field direction. An electron-electron interaction mediates a coupling among them, giving rise to a generic $2k_F$ instability toward various spontaneous symmetry breaking (SSB) phases such as charge density wave, spin density wave and Wigner crystal phases¹⁻⁸. In expectation of these phases, high magnetic field transport experiments have been carried out during last a few decades in semimetal materials with dilute electron densities, where smaller magnetic fields enable us to reach the (quasi) quantum limit. These experimental efforts lead to discoveries of unusual consecutive metal-insulator transitions in graphite above the quasi quantum limit⁹⁻¹⁷, first-order phase transition into a phase with larger magnetic anisotropy in bismuth¹⁸⁻²⁰, and an abrupt field-induced quantum phase transition in Weyl semimetals such as tantalumn phosphide^{21,22}. Previous theories^{2-8,23-29} studied possible SSB phases in (some of) these systems by means of energy estimations as well as functional renormalization group analyses. Meanwhile, few theories³⁰ have been done on transport properties of respective SSB phases, which hinder us from deciphering identities of the low-temperature phases in the experiments.

In this paper, we present a theory of transport properties of density wave (DW) phases in a 3D electron gas under a high magnetic field. The DW phases considered in this paper break the translational symmetry along the field direction, and can be regarded as a canonical example of SSB phases in 3D metals/semimetals under the high field^{3,8,23-25,27,30}. The quasi-one-dimensional electronic system with an electron interaction is transformed

to an effective boson model, which takes a form of coupled one-dimensional wires of Luttinger liquids. Using a renormalization group study, we first observe that, in the case of an repulsive electron-electron interaction, the model exhibits a finite temperature phase transition as well as a $T = 0$ quantum phase transition between a normal phase and the DW phase. Using the boson model, we next calculate longitudinal optical conductivities in the DW phases with inclusions of charge fluctuation (phason excitation) effect and impurity (disorder) effect. When regularized into a lattice, a partition function of the effective boson Hamiltonian can be seen as that of a classical 3D XY model, while the imaginary-time single-particle *electron* Green function can be seen as a partition function of the XY model in the presence of two pairs of magnetic dipoles. By employing the celebrated duality mapping³¹⁻³³, we evaluate the single-particle electron Green function and spectral function in the DW and normal phases. The optical conductivity and spectral function thus calculated acquire continuum spectral weights in low-frequency regime in the DW phases, which reflect the presence of the phason excitations. We show that, in the presence of a bulk-surface coupling, the finite spectral weight in the single-particle spectral function in *bulk* electronic states can be transferred into that of the chiral *surface* Fermi arc states. We further argue that this results in a temperature-dependent in-plane surface conductance, providing a possible explanation for a recent transport experiment in graphite¹⁶.

A. highlight of this paper

Using the one-dimensional bosonization scheme³⁴, we first bosonize an electron Hamiltonian with a repulsive electron-electron interaction. The boson Hamiltonian takes a form of coupled one-dimensional chains. Each one-dimensional system is described by a quantum sine-Gordon model with a pair of two conjugate phase vari-

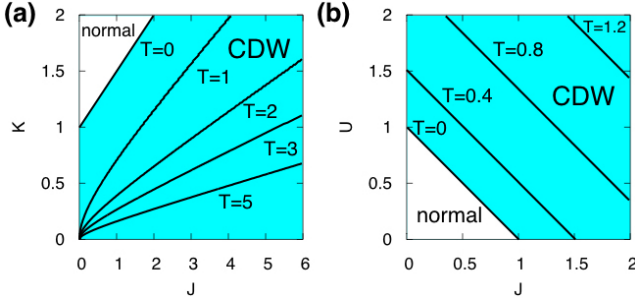


FIG. 1. (color online) Contour map of three-dimensional phase diagrams subtended by (a) J , K (Luttinger parameter) and T (temperature) at general electron filling and (b) J and U (umklapp term), and T at half electron filling for $K = 1.5 > K_c (= 1)$. Phase boundaries between normal phase (white color region at $T = 0$) and DW phase (blue region) are depicted by black curves at different temperatures (read the text for units of J, U, K and T).

ables, an electron displacement field $\phi_j(z)$ (along the field direction) and electron current field $\Pi_j(z)$,

$$H = \sum_m \int dz \left\{ \frac{uK\pi}{2} [\Pi_m(z)]^2 + \frac{u}{2\pi K} [\partial_z \phi_m(z)]^2 - \sum_{j \neq m} J_{j-m} \sigma_j^z \sigma_m^z \cos 2[\phi_j(z) - \phi_m(z)] \right\}, \quad (1)$$

where j denotes the chain index ($j, m = 1, 2, \dots, \frac{S}{2\pi l^2}$ with a magnetic length l and an area of the system perpendicular to the field S). K and u stand for Luttinger parameter and renormalized velocity for each one-dimensional chain, while σ_j^z is an Ising variable associated with two Klein factors for left and right movers. Due to the repulsive interaction, displacement fields in different chains are coupled with each other ferromagnetically;

$$J_m \equiv \frac{\sqrt{2\pi}l}{L_x} J e^{-\frac{y_m^2}{2l^2}}, \quad (2)$$

with $J > 0$ and $y_m \equiv 2\pi l^2 m / L_x$ ($m = 1, 2, \dots$). The inter-chain coupling ranges over the magnetic length l , within which $\mathcal{O}(L_x/l)$ number of chains are ferromagnetically coupled with one another ('long-range' coupling; L_x is a linear dimension of a system size). Due to this inter-chain rigidity, the displacement field naturally exhibits a long range order at lower temperature or for smaller Luttinger parameter (Fig. 1). The order is nothing but the DW order which breaks spontaneously the translational symmetry along the field direction. At general (incommensurate) electron filling case, where $2k_F$ along the field direction is incommensurate to a reciprocal lattice vector along the field, the DW order breaks a continuous $U(1)$ translational symmetry. The DW phase is accompanied by a gapless Goldstone mode, i.e. phason excitation.

Based on this boson model, we calculate the conductivity in the DW phase by taking into account effects of

phason excitation and disorder potential. The conductivity in the clean limit shows a Drude peak at $\omega = 0$ at the incommensurate electron filling case, $\text{Re}\sigma_{zz}(\omega) = 2A\delta(\omega)$ with $A = e^2 u K / (2\pi l^2)$. The Drude peak at $\omega = 0$ represents the gapless nature of the phason excitation.

At a commensurate electron filling case, where $2k_F$ along the field direction is commensurate to the reciprocal lattice vector, the interaction part allows a umklapp process, which adds a phase locking term into the effective boson Hamiltonian. For the half filling case, for example, the term takes a form of

$$H_u \equiv - \sum_{j,m} U_{j-m} \sigma_j^z \sigma_m^z \int dz \cos 2[\phi_j(z) + \phi_m(z)], \quad (3)$$

$$U_m \equiv \frac{\sqrt{2\pi}l}{L_x} U e^{-\frac{y_m^2}{2l^2}}. \quad (4)$$

These phase locking terms lock the displacement field on discrete values, reducing a symmetry of the Hamiltonian from $U(1)$ to Z_n for the m/n electron filling cases respectively (m, n are mutually prime integers). Due to these phase locking terms, the phason excitation in the DW phase acquires a finite mass, splitting the Drude peak at $\omega = 0$ into two resonance peaks at $\omega = \omega_U$, $\text{Re}\sigma_{zz}(\omega) = A\delta(|\omega| - \omega_U)$ with $\omega_U = \sqrt{8\pi u K U}$, where U stands for the strength of the umklapp term.

In the presence of finite disorder, the optical conductivity further acquires a *continuum spectrum* above a threshold frequency (Fig. 2(a)). It takes a form of

$$\overline{\text{Re}\sigma_{zz}(\omega)} = \frac{2A}{\pi} \frac{\bar{g}_y}{\sqrt{\omega^2 - \omega_J^2}} \frac{|\omega| \Theta(|\omega| - \omega_J)}{\omega^4 + \bar{g}_y^2 / (\omega^2 - \omega_J^2)}, \quad (5)$$

with $\omega_J \equiv \sqrt{4\pi u K J}$ in the DW phase at incommensurate electron filling case. J and \bar{g}_y stand for the inter-chain coupling strength and disorder strength respectively. Remark that the Drude peak in the clean limit diminishes immediately once an infinitesimally small \bar{g}_y is introduced.

In the DW phase at the commensurate filling, the conductivity also acquires a continuum spectrum above a threshold frequency (Fig. 2(b)),

$$\overline{\text{Re}\sigma_{zz}(\omega)} = \frac{2A\omega_0}{|F'_-(\omega_0)|} \delta(|\omega| - \omega_0) + \frac{2A}{\pi} \frac{\bar{g}_y}{\sqrt{\omega^2 - \omega_c^2}} \times \frac{|\omega| \Theta(|\omega| - \omega_c)}{(\omega^2 - \omega_U^2)^2 + \bar{g}_y^2 / (\omega^2 - \omega_c^2)}, \quad (6)$$

with the threshold frequency $\omega_c^2 \equiv \omega_J^2 + \omega_U^2 / 2$. Unlike the incommensurate filling case, the resonance mode in the clean limit survives even in the presence of finite (but small) disorder; the first term in the right hand side of eq. (6). The location of the mode (a renormalized mass ω_0) is determined as a root of a monotonically-decreasing function,

$$F_-(\omega_0) = 0, \\ F_-(\omega) \equiv -\omega^2 + \omega_U^2 - \frac{\bar{g}_y}{\sqrt{\omega_c^2 - \omega^2}}. \quad (7)$$

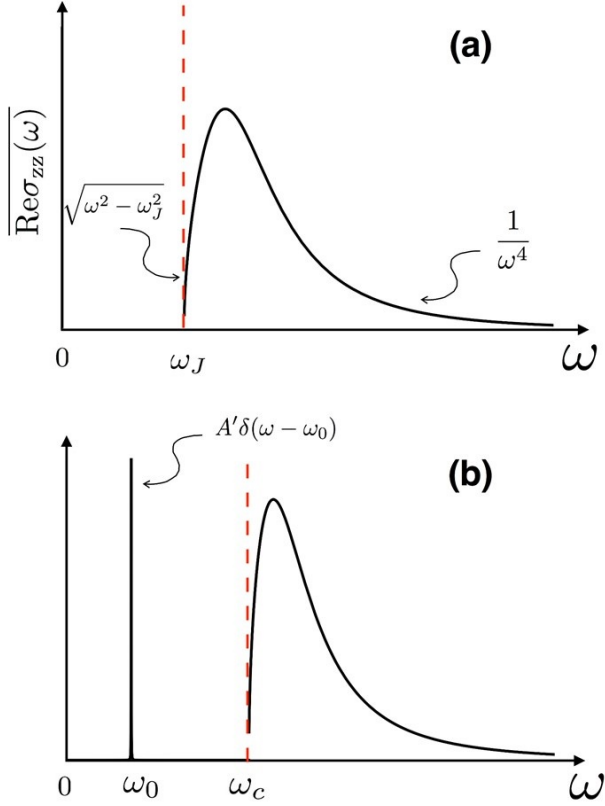


FIG. 2. (color online) disorder-averaged optical conductivity $\text{Re}\sigma_{zz}(\omega)$ as a function of frequency ω . The threshold frequencies are labeled by red dashed lines, above which the conductivity shows a continuum spectrum. (a) DW phase at incommensurate electron filling case. (b) DW phase at commensurate electron filling case (weak disorder case, $\bar{g}_y < \bar{g}_{y,c}$; see the text). Note that the resonance mode at $\omega = \omega_U$ in the clean limit is shifted to $\omega = \omega_0$ due to a renormalization by a finite disorder \bar{g}_y . $A' \equiv 2A/|F'_-(\omega_0)|$ where $A \equiv e^2 u K / (2\pi l^2)$ and $F'_-(\omega)$ and ω_0 are defined by eq. (7).

On increasing the disorder strength \bar{g}_y , the mass becomes smaller. Within the Born approximation, there is a critical disorder strength $\bar{g}_{y,c} \equiv \omega_{UJ}^2 \omega_c$, at which the renormalized mass ω_0 becomes zero and above which the resonance mode diminishes. This critical point clearly suggests a quantum phase transition from the DW phase to a disorder-driven phase.

The optical conductivity shown in Fig. 2 reflects a nature of low-energy collective mode (phason excitation) in the DW phases. The fluctuation of the displacement and current fields constitute the collective mode, which has an energy-momentum dispersion relation $E(k_z, k)$. k_z and k are momenta conjugate to z (spatial coordinate along the field) and the chain index or coordinate (a spatial coordinate perpendicular to the field) respectively. Due to the ‘long-range’ inter-chain coupling, *all* the collective modes with finite k have a finite mass at $k_z = 0$ in the

thermodynamic limit;

$$E(k_z = 0, k \neq 0) = \begin{cases} \omega_J & \text{incommensurate,} \\ \omega_c & \text{commensurate.} \end{cases} \quad (8)$$

With disorder, these finite- k phason modes contribute to the continuum spectrum above the threshold frequency. Meanwhile, the phason mode at $k = 0$ has no mass in the incommensurate filling case and has a finite mass in the commensurate filling case;

$$E(k_z = 0, k = 0) = \begin{cases} 0 & \text{incommensurate,} \\ \omega_U \text{ (or } \omega_0) & \text{commensurate.} \end{cases} \quad (9)$$

The phason mode at $k = 0$ contributes to the Drude peak in the incommensurate filling case and the resonance peak in the commensurate filling case respectively.

The low-energy phason mode induces a strong charge fluctuation, so that it may dramatically modify a naive ‘mean-field’ picture of the single-electron excitation spectrum in the DW phase. To explore this possibility, we calculate the single-particle spectrum function in terms of the boson Hamiltonian. We first note that the $T = 0$ partition function of the bosonized Hamiltonian can be described by a classical XY model in a cubic lattice, while a single-particle imaginary time Green function can be described by a partition function of the 3D XY model in the presence of two pairs of magnetic monopole and antimonopoles. A U(1) phase degree of freedom of the XY model corresponds to the displacement field along the field, so that ordered/disordered phases in the XY model correspond to the DW/normal phases near the DW phase transition respectively.

Using the celebrated duality mapping between the XY and frozen lattice superconductor (FLS) models^{31–33}, we calculate an asymptotic behavior of the single-particle imaginary-time Green function in the DW/normal phases. After an analytic continuation, we obtain the single-particle real-time Green function, whose imaginary part is nothing but the single-particle spectral function. In the DW phase, the spectral function thus obtained takes a form of

$$\rho_\sigma(q_z, \omega) = \frac{B}{\sqrt{\omega^2 - u^2 q_z^2}} \Theta(|\omega| - u|q_z|) + \dots \quad (10)$$

with small $q_z = k_z - \sigma k_F$ near the two Fermi points. $\sigma = \pm$ specifies one of the two Fermi points. For the normal phase at the incommensurate filling, the spectral function is given by

$$\rho_\sigma(q_z, \omega) = B' \sqrt{\omega^2 - u^2 q_z^2} \Theta(|\omega| - u|q_z|) + \dots \quad (11)$$

where B and B' are non-universal parameters. As shown in Fig. 3(a), the spectral functions in both phases have structures at $\omega = \pm u q_z$ with power-law behaviors. The result clearly shows that, due to the strong phase fluctuation, the single-particle spectral functions in DW/normal phases acquire low-energy continuum spectra at;

$$|\omega| > u|k_z - \sigma k_F| \quad (12)$$

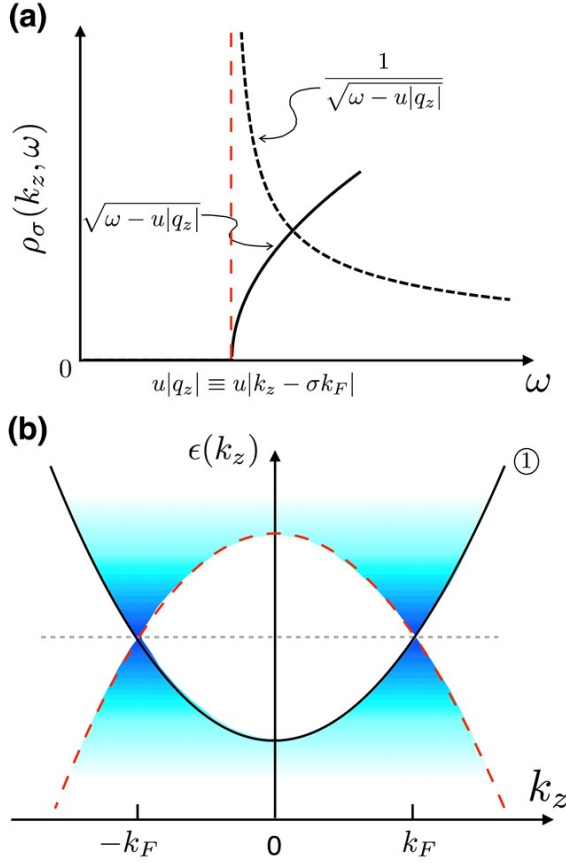


FIG. 3. (a) Bulk single-particle spectral functions $\rho_\sigma(k_z, \omega)$ near the two Fermi points ($k_z = \pm k_F$) in the DW phase (dotted line) and for the normal phase (solid line) for the incommensurate electron filling case. $\sigma = \pm$ specifies one of the two Fermi points; $k_z = \sigma k_F$. u is a renormalized velocity (see the text). (b) Schematic picture of an energy-momentum dispersion for a bulk single-particle state $\epsilon_b(k_z) = \hbar^2 k_z^2 / (2m_*)$ (①) and dissipative region (defined by Eqs. (12,13); blue color region). m_* denotes an effective electron mass and straight dotted horizontal line stands for the Fermi energy μ , which defines the two Fermi points in the bulk at $k_z = \pm k_F$. $\epsilon_b(k_z)$ and $2\mu - \epsilon_b(k_z)$ (red dotted curved line) bound the dissipative region. Within the dissipative region, the single-particle spectral function acquires finite continuum weight as in Fig. 3(a).

with $\sigma = \pm$. More generally, the region can be seen as the low-energy limit of the following energy-momentum region;

$$|\omega| > |\epsilon_b(k_z) - \mu|. \quad (13)$$

$\epsilon_b(k_z)$ denotes the one-dimensional electronic dispersion along the field direction, e.g. $\epsilon_b(k_z) = \hbar^2 k_z^2 / (2m_*)$ with effective electron mass m_* . We dub this region as ‘dissipative regime’ (a blue-colored region in Fig. 3(b)).

As an application of our finding above, we consider an in-plane surface conductance in the DW/normal phase near the phase transition. The in-plane conductance (in

xy plane) at temperature lower than the cyclotron frequency can be dominated by surface transport rather than bulk transport (at least in the clean limit). The bulk electronic state forms two parallel Fermi lines at $k_z = \pm k_F$ in a two-dimensional plane subtended by k_z and the chain coordinate. The two are connected with each other by Fermi arc states at the surface regions (Figs. 4(a,b,c)). The arc states have chiral dispersions, and can be regarded as a bundle of chiral edge modes (chiral surface state or chiral surface Fermi arc state^{1,35,36}). The DW order removes the two Fermi lines, while keeps intact the arc states except for their two end points (Fig. 4(d)). The two end point states repel each other by the $2k_F$ nesting vector, such that the Fermi arc state at $k_z = k_F$ is continuously connected to the state at $k_z = -k_F$. This leads to a perfect disconnection between the arc state at one boundary and that at the other side of the boundary. Therefore, one may naively expect that the arc states provide a robust in-plane conductance.

Contrary to this naive expectation, however, we show that a finite surface-bulk coupling transfers the low-energy continuum spectral weight in the bulk state into the surface Fermi arc state, causing a *finite life time* to those arc states in the dissipative region. Using the Landauer formula, we show that, due to this finite life time, the in-plane surface conductance acquire a temperature dependence as;

$$G_s = \frac{e^2}{h} \sum_{k_z} \left(1 - \frac{1}{e^{\beta|\epsilon_b(k_z) - \mu|} + 1} \right), \quad (14)$$

where the summation over k_z is taken over $[-k_F, k_F]$. At the zero temperature, the surface conductance takes a quantized value ($N_z e^2 / h$; N_z is a number of chiral edge modes), as all the surface Fermi arc states on the chemical potential are outside the dissipative region (see Fig. 5). Nonetheless, the arc states in the dissipative region are thermally activated at finite temperature, which leads to a reduction of the surface conductance as in eq. (14). We believe that the derived expression could provide a possible explanation of an unusual ‘in-plane metallic behavior’, as observed in one of the two SSB phases in graphite.

B. structure of this paper

The structure of this paper is as follows. In the next section (Sec. II), we introduce an interacting electron model, its effective boson Hamiltonian, and a phase diagram obtained from the renormalization group (RG) study. Using the boson Hamiltonian, we calculate in Sec. III the longitudinal (optical) conductivities in the density wave phases with disorders. In Sec. IV, we employ a lattice-regularized version of the effective boson model (3D XY model), to calculate the single-particle spectral function by way of the electromagnetic duality map between XY and FLS models. In Sec. V, we argue that the chiral surface Fermi arc states can generally

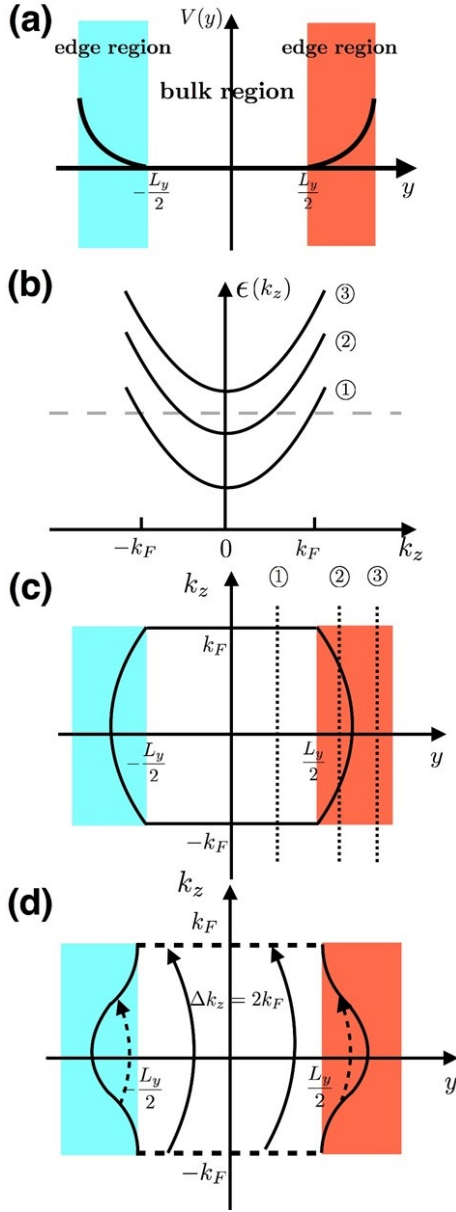


FIG. 4. (a) Confining potential along the y direction; $V(y)$. $V(y) = 0$ in a bulk region ($|y| < L_y/2$), while $V(y) > 0$ in edge (surface) regions ($|y| > L_y/2$). (b) Schematic picture of electronic energy dispersion for a single particle state in the bulk $\epsilon_b(k_z) = \hbar^2 k_z^2 / (2m_*)$ (①) and that localized at $y = y_j$ with $|y_j| > L_y/2$ (②, ③); $\epsilon_{s,j}(k_z) = \hbar^2 k_z^2 / (2m_*) + V(y_j)$. The subscript ‘b’ and ‘s’ stand for ‘bulk’ and ‘surface’ respectively. The subscript ‘j’ stands for the chain index linked with y_j as $y_j \equiv 2\pi j l^2 / L_x$ (L_x is a linear dimension along the x -direction). The single-particle energy in the edge (surface) region acquires an energy shift due to the confining potential $V(y_j)$. The energy shift moves two Fermi points inward, forming a Fermi arc state in the edge (surface) regions. (c) Two parallel Fermi lines in the bulk and Fermi arc states which connect them. ①, ②, ③ in Fig. (c) correspond to ①, ②, ③ in Fig. (b) respectively. (d) Fermi arc states in the presence of the density wave order in the bulk.

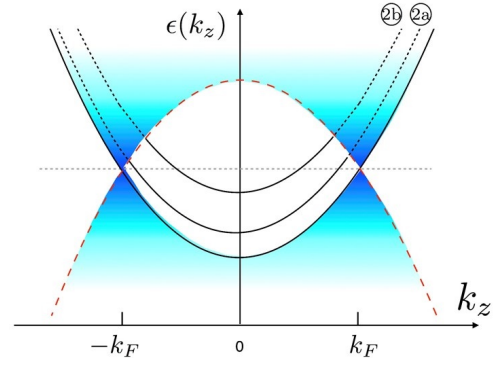


FIG. 5. Schematic picture of the dissipative region and the energy-momentum dispersion for the surface single-particle states localized at the edge (surface) regions (2a, 2b). The surface states in the dissipative region (dotted curve parts) acquire a finite life time due to a surface-bulk coupling.

have a finite life time due to a surface-bulk coupling. We further discuss the temperature-dependence of in-plane conductance due to the chiral surface states. Sec. VI is devoted to conclusion and outlook. For completeness, we review how an interacting electron Hamiltonian is bosonized into coupled quantum sine-Gordon models (appendix A). We give in appendix B a derivation of the finite-temperature RG equation for the effective boson Hamiltonian. Detailed procedures of the conductivity calculation and of the spectral function calculation are given in appendix C and D respectively.

II. HAMILTONIAN, BOSONIZATION AND A RG PHASE DIAGRAM

We consider a 3D isotropic metal with parabolic energy band dispersion under high magnetic field along the z -direction. The kinetic energy part is given by

$$\begin{aligned} \mathcal{H}_{\text{kin}} &= \int d\mathbf{r} \Psi^\dagger(\mathbf{r}) \left(\frac{\pi^2}{2m_*} - \mu \right) \Psi(\mathbf{r}) \\ &= \sum_{n, k_z, j} \left(\frac{\hbar^2 k_z^2}{2m_*} + \left(n + \frac{1}{2} \right) \hbar \omega_0 - \mu \right) c_{n,j,k_z}^\dagger c_{n,j,k_z}, \end{aligned} \quad (15)$$

with $\pi \equiv -i\hbar(\nabla_x - ieBy, \nabla_y, \nabla_z)$, an effective mass of electron m_* , momentum along the field direction k_z , the cyclotron frequency $\hbar\omega_0 \equiv eB/m_*$, Landau level index n . j (what we will call the ‘chain index’ later) denotes degeneracy within each Landau level; $j = 1, 2, \dots, L_x L_y / (2\pi l^2)$ and magnetic length $l \equiv \sqrt{\hbar/(eB)}$. L_x and L_y are linear dimensions of the system size along the x and y -direction respectively. c_{n,j,k_z}^\dagger is a creation operator for the n -th Landau level with j and k_z . In the Landau gauge, the electron creation operator can be

expanded by the corresponding single-particle state as;

$$\Psi^\dagger(\mathbf{r}) \equiv \sum_{n,j,k_z} \varphi_{n,j,k_z}^*(\mathbf{r}) c_{n,j,k_z}^\dagger \quad (16)$$

$$\varphi_{n,j,k_z}(\mathbf{r}) \equiv \frac{e^{ik_x x + ik_z z - (y-y_j)^2/2l^2}}{\sqrt{\sqrt{\pi}lL_xL_z}} \frac{H_n((y-y_j)/l)}{\sqrt{2^n n!}} \quad (17)$$

with $\mathbf{r} \equiv (x, y, z)$, $k_x \equiv 2\pi j/L_x$, $y_j \equiv 2\pi l^2 j/L_x$ and the Hermite polynomial $H_n(y)$. For simplicity, we consider the spinless case. We put the chemical potential μ in the lowest Landau level (LLL) and assume that $\hbar\omega_0$ is larger than the largest kinetic energy along the field direction. We linearize the quadratic energy dispersion around the two Fermi points $k_z = \pm k_F$. This leads to a Hamiltonian for a slowly-varying field operator $\psi_{\sigma,j}(z)$ (defined below),

$$\mathcal{H}_{\text{kin}} = \sum_{j,\sigma=\pm} \int dz \sigma v_F \psi_{\sigma,j}^\dagger(z) i \partial_z \psi_{\sigma,j}(z) + \dots, \quad (18)$$

with a bare Fermi velocity $v_F \equiv \hbar k_F/m_*$, Fermi wavelength k_F . We take $\hbar = 1$ henceforth. $\sigma = \pm$ specifies one of the two Fermi points,

$$\begin{aligned} \Psi^\dagger(\mathbf{r}) &\equiv \frac{1}{\sqrt{\sqrt{\pi}lL_x}} \sum_j e^{-ik_x x - (y-y_j)^2/2l^2} \psi_j^\dagger(z) + \dots, \\ \psi_j^\dagger(z) &\equiv e^{-ik_F z} \psi_{+,j}^\dagger(z) + e^{ik_F z} \psi_{-,j}^\dagger(z). \end{aligned} \quad (19)$$

For the interaction part, we consider a short-ranged electron-electron interaction among the LLL electrons;

$$\begin{aligned} \hat{\mathcal{H}}' &= \int d^3\mathbf{r} \int d^3\mathbf{r}' V(\mathbf{r} - \mathbf{r}') \Psi^\dagger(\mathbf{r}) \Psi^\dagger(\mathbf{r}') \Psi(\mathbf{r}') \Psi(\mathbf{r}) \\ &= \frac{g}{L_x} \int dz \int dz' \sum_{j,m,n} V_{m-n,j-n}(z, z') \\ &\quad \times \hat{\psi}_n^\dagger(z) \hat{\psi}_{j+m-n}^\dagger(z') \hat{\psi}_m(z') \hat{\psi}_j(z) + \dots \end{aligned} \quad (20)$$

with

$$\begin{aligned} V_{m-n,j-n}(z, z') &= \\ \frac{1}{(2\pi)^2 l_0 l'} e^{-\frac{(z-z')^2}{2l_0^2} - \frac{(y_j-y_n)^2}{2l^2} - \frac{(y_n-y_m)^2}{2(l^2+l_0^2)}} \end{aligned} \quad (22)$$

for a short-range interaction potential^{27,34}

$$V(\mathbf{r} - \mathbf{r}') = \frac{g}{(\sqrt{2\pi}l_0)^3} e^{-\frac{|\mathbf{r}-\mathbf{r}'|^2}{2l_0^2}} \quad (23)$$

with an interaction length l_0 and $l'^2 \equiv l_0^2 + l^2$.

We bosonize the fermion field for each single-particle state localized at y_j as,

$$\psi_{\sigma,j}(z) = \frac{\eta_{\sigma,j}}{\sqrt{2\pi\alpha}} e^{-i(\sigma\phi_j(z) - \theta_j(z))},$$

where an electron displacement field $\phi_j(z)$ and current field $\partial_z \theta_j(z)$ are conjugate to each other,

$$[\phi_j(z), \partial_{z'} \theta_m(z')] = i \delta_{j,m} \delta(z - z').$$

$\eta_{\sigma,j}$ is the Klein factor (Majorana fermion) ensuring the anticommutation between two fermion fields on different j and σ ; $\{\eta_{\sigma,j}, \eta_{\sigma',m}\} = \delta_{\sigma,\sigma'} \delta_{j,m}$. α defines a short-range cutoff for the spatial coordinate z ³⁴. Due to the Klein factor, the interaction part cannot be fully bosonized without approximation.

To obtain an effective field theory description for the density wave ordering, we employ random phase approximation, keeping only the Hartree term ($j = n$) and Fock term ($m = n$) in \mathcal{H}' . This leads to a bosonized Hamiltonian (Appendix A),

$$\begin{aligned} H &= \sum_m \int dz \left\{ \frac{uK\pi}{2} [\Pi_m(z)]^2 + \frac{u}{2\pi K} [\partial_z \phi_m(z)]^2 \right. \\ &\quad \left. - \sum_{j \neq m} J_{j-m} \sigma_j^z \sigma_m^z \cos 2[\phi_j(z) - \phi_m(z)] \right\}, \end{aligned} \quad (24)$$

$$J_m \equiv \frac{\sqrt{2\pi}l}{L_x} J e^{-\frac{y_m^2}{2l^2}}, \quad (25)$$

with $y_m \equiv 2\pi l^2 m/L_x$ and $\pi \Pi_j \equiv \partial_z \theta_j(z)$, Luttinger parameter K and renormalized velocity u . Ising variable $\sigma_m^z = \pm 1$ is associated with the Klein factors of left and right mover for each m ; $\sigma_m^z \equiv i\eta_{+,m}\eta_{-,m}$. The Fock term combined with the Hartree term give a positive J_{j-m} in total, which gives a rigidity between the displacement field on j and that on m . Since the bosonized Hamiltonian resembles that of coupled one-dimensional systems ('chains'), let us refer to j, m as *chain* index. The inter-chain rigidity ranges over the magnetic length, within which $\mathcal{O}(L_x/l)$ -number of chains are ferromagnetically coupled with one another. In the thermodynamic limit ($L_x \rightarrow \infty$), the number of chains within l becomes infinite ('infinite-range' coupling). Due to the inter-chain rigidity, a long range order sets in for smaller K and lower temperature, $\langle \phi_j(z) \rangle = \phi$. The order is a charge density wave order, which breaks the translational symmetry along z .

For a half electron filling, where $2k_F$ is half of a reciprocal lattice vector along z , the interaction part allows a umklapp process, which adds a phase locking term into eq. (24);

$$H_u \equiv - \sum_{j,m} U_{j-m} \sigma_j^z \sigma_m^z \int dz \cos 2[\phi_j(z) + \phi_m(z)], \quad (26)$$

$$U_m \equiv \frac{\sqrt{2\pi}l}{L_x} U e^{-\frac{y_m^2}{2l^2}}. \quad (27)$$

The added term with the rigidity term locks the displacement fields on discrete values, $\langle \phi_j(z) \rangle = 0, \pi/2, \pi, \dots$ for positive U . The umklapp term reduces a symmetry of the Hamiltonian from $U(1)$ to Z_2 ; low-energy collective excitation in the charge density wave phase acquires a mass.

For larger Luttinger parameter/temperature T , quantum/thermal fluctuation may destroy the density wave order. To see this, we derive renormalization group (RG) flow equations for coupling constants (appendix B);

$$\frac{dJ}{dl} = \left[2 - 2K \coth \frac{\Lambda}{2T}\right] J + KC[J^2 + U^2], \quad (28)$$

$$\frac{dU}{dl} = \left[2 - 2K \coth \frac{\Lambda}{2T}\right] U + 2KCJU, \quad (29)$$

with $dT/dl = T$,

$$J \equiv \sum_m J_m, \quad U \equiv \sum_m U_m. \quad (30)$$

C is a numerical constant and Λ is an ultraviolet energy cutoff. The Luttinger parameter K is not renormalized in the leading order expansion in $1/L_x$. For general electron filling case ($U = 0$) and at $T = 0$, the Luttinger parameter has a critical value $K_c (= 1)$ above/below which small inter-chain rigidity J is irrelevant/relevant (normal/DW phase) respectively (Fig. 1). For finite T , small inter-chain rigidity is renormalized to zero for any K , while J above a critical strength increases on renormalization. The RG equations also suggest that the umklapp term and inter-chain rigidity term always help each other to grow into larger values for positive J , while small umklapp term is renormalized to zero for negative J (Fig. 1).

III. LONGITUDINAL CONDUCTIVITY IN DENSITY WAVE PHASES

A. conductivity in the presence of disorders

According to the linear response theory, longitudinal conductivity along the field direction is given by a retarded correlation function between an electric current operator and electric polarization operator,

$$\sigma_{zz}(\omega) = -\frac{i}{V} \int_{-\infty}^{\infty} dt \Theta(t) e^{i\omega t} \text{Tr} \left[\hat{\rho}_G [e^{i\hat{K}t} \hat{J}_z e^{-i\hat{K}t}, \hat{P}_z] \right]. \quad (31)$$

V is the volume of the system; $V \equiv L_z L_x L_y$. The electric current \hat{J}_z and polarization \hat{P}_z are given by the two phase variables;

$$\hat{J}_z = \frac{|e|uK}{\pi} \sum_j \int dz \partial_z \hat{\theta}_j(z), \quad (32)$$

$$\hat{P}_z = -\frac{|e|}{\pi} \sum_j \int dz \hat{\phi}_j(z). \quad (33)$$

\hat{K} and $\hat{\rho}_G$ in Eq. (31) are Hamiltonian and a statistical density operator respectively (see Eqs. (34,38,39) for their definitions of our actual calculations).

The displacement field exhibits a long range order in the density wave (DW) phases, $\langle \hat{\phi}_j(z) \rangle = \phi_0$. The

quantum fluctuation around the DW order can be described by a linear combination of the current density field $\hat{\Pi}_j(z) \equiv \frac{1}{\pi} \partial_z \hat{\theta}_j(z)$ and small fluctuations of the displacement field from its ordered value $\hat{\chi}_j(z) \equiv \hat{\phi}_j(z) - \phi_0$. An expansion of the bosonized Hamiltonian Eqs. (24,26) with respect to these fluctuations up to the second order leads to a spin-wave Hamiltonian (gaussian approximation),

$$\begin{aligned} H_{\text{sw}} = & \frac{1}{2\pi} \sum_j \int dz \left\{ uK (\partial_z \hat{\theta}_j(z))^2 + \frac{u}{K} (\partial_z \hat{\chi}_j(z))^2 \right\} \\ & + \sum_{j,m} 2J_{j-m} \int dz (\hat{\chi}_j(z) - \hat{\chi}_m(z))^2 \\ & + \sum_{j,m} 2U_{j-m} \int dz (\hat{\chi}_j(z) + \hat{\chi}_m(z))^2. \end{aligned} \quad (34)$$

Here $U_{j-m} = 0$ for the DW phase in the incommensurate electron filling case. Correspondingly, the displacement field operator $\hat{\phi}_j(z)$ in eq. (33) is replaced by $\hat{\chi}_j(z)$ henceforth. Note that we have omitted the Ising variables σ_z^j from Eqs. (24,26). This is because the DW states are described by $\sigma_z^j = +1$ for all j (or by $\sigma_z^j = -1$ for all j), and because small fluctuations around them are not accompanied by flipping these Ising variables. Note also that the following argument at the half filling case can be generalized to other commensurate electron filling cases.

Electronic disorder potentials are coupled with the displacement field and are generally given by

$$H_{\text{imp}} = \sum_{n=1,2,\dots} \sum_j \int dz A_{j,(n)}(z) \cos(2n\hat{\phi}_j(z) + \lambda_{j,(n)}(z)). \quad (35)$$

Here a cosine term with $n = 1$ comes from a single-particle backward scattering process

$$H_{\text{imp}}^{(1)} = \sum_j \int dz A_{j,(1)}(z) \{ e^{i\lambda_{j,(1)}(z)} \hat{\psi}_{+,j}^\dagger(z) \hat{\psi}_{-,j}(z) + \text{h.c.} \}$$

while a cosine term with $n = 2$ comes from two-particle backward scattering process,

$$\begin{aligned} H_{\text{imp}}^{(2)} = & \sum_{j,m} \int dz A_{j,m,(2)}(z) \{ e^{i\lambda_{j,m,(2)}(z)} \\ & \times \hat{\psi}_{+,j}^\dagger(z) \hat{\psi}_{+,m}^\dagger(z) \hat{\psi}_{-,m}(z) \hat{\psi}_{-,j}(z) + \text{h.c.} \}. \end{aligned}$$

It is natural to expect that these backward scattering disorders have significant impact on the transport properties. To see their effect on the conductivity, H_{imp} is further expanded up to the second order in the fluctuation of the displacement field;

$$H_{\text{imp}} = \sum_j \int dz (X_j(z) \hat{\chi}_j(z) + Y_j(z) \hat{\chi}_j^2(z)) + \mathcal{O}(\chi^3). \quad (37)$$

Here $X_j(z)$ and $Y_j(z)$ are given by random amplitudes $A_{j,(n)}(z)$ and random phases $\lambda_{j,(n)}(z)$;

$$X_j(z) \equiv 2 \sum_{n=1,2,\dots} n A_{j,(n)}(z) \sin(2n\phi_0 + \lambda_{j,(n)}(z)),$$

$$Y_j(z) \equiv 2 \sum_{n=1,2,\dots} n^2 A_{j,(n)}(z) \cos(2n\phi_0 + \lambda_{j,(n)}(z)).$$

We first calculate the conductivity from Eq. (31) with

$$\hat{K} = \hat{H}_{\text{sw}} + \sum_j \int dz (X_j(z) \hat{\chi}_j(z) + Y_j(z) \hat{\chi}_j^2(z)), \quad (38)$$

$$\hat{\rho}_G = e^{-\beta \hat{K}} / \text{Tr}[e^{-\beta \hat{K}}]. \quad (39)$$

Then we take quenched average over random amplitudes $A_{j,(n)}(z)$ and random phases $\lambda_{j,(n)}(z)$ by

$$\overline{\dots} = \frac{\int \mathcal{D}X_j(z) \mathcal{D}Y_j(z) \dots e^{-\frac{1}{g_x} \sum_j \int dz X_j^2(z) - \frac{1}{g_y} \sum_j \int dz Y_j^2(z)}}{\int \mathcal{D}X_j(z) \mathcal{D}Y_j(z) e^{-\frac{1}{g_x} \sum_j \int dz X_j^2(z) - \frac{1}{g_y} \sum_j \int dz Y_j^2(z)}}. \quad (40)$$

g_x and g_y stand for disorder strengths associated with disordered fields $X_j(z)$ and $Y_j(z)$ respectively. We take the disorder average of the conductivity within a Born approximation, to obtain

$$\overline{\sigma_{zz}(\omega)} = \overline{Q_{zz}(i\omega_n = \omega + i\eta)}, \quad (41)$$

$$\overline{Q_{zz}(i\omega_n)} = \frac{e^2 u K}{\pi^2 l^2} \times \frac{\omega_n}{\omega_n^2 + 2u\pi K U(0) - \frac{2\pi u K g_y}{L_z N} \sum_{\mathbf{k}} [M_0^{-1}(\mathbf{k}, \omega_n)]_{2,2}}, \quad (42)$$

with

$$[M_0^{-1}(\mathbf{k}, \omega_n)]_{2,2} = \frac{\pi u K}{E^2(k_z, k) + \omega_n^2}, \quad (43)$$

$$E(k_z, k) = \sqrt{u^2 k_z^2 + 2u\pi K (J(k) + U(k))}. \quad (44)$$

$Q_{zz}(i\omega_n)$ is a Fourier-transform of imaginary-time correlation function between the current density and displacement field (see Appendix C) and $i\omega_n$ is Matsubara frequency $i\omega_n = 2\pi n/\beta$ with temperature β^{-1} . $\mathbf{k} \equiv (k_z, k)$ and k_z and k are momenta conjugate to the coordinate along the field direction z and coordinate associated with the chain index y_j respectively. For example, a Fourier transformation of $\chi_j(z)$ is given by

$$\chi_j(z) = \frac{1}{L_z N} \sum_{\mathbf{k}} e^{ik_z z + ik y_j} \chi(\mathbf{k}),$$

with $N \equiv L_x L_y / (2\pi l^2)$. $J(k)$ and $U(k)$ in eq. (44) are given by Fourier transforms of J_j and U_j with respect to

the chain coordinate y_j ;

$$J(k) \equiv \sum_{n=1}^N J_n |1 - e^{iky_n}|^2, \quad (45)$$

$$U(k) \equiv \sum_{n=1}^N U_n |1 + e^{iky_n}|^2. \quad (46)$$

$$U(k) \equiv \sum_{n=1}^N U_n |1 + e^{iky_n}|^2. \quad (47)$$

B. Low-energy collective excitations in density wave phases

Low-energy collective excitations in the DW phases consist of fluctuations of current and displacement field. They are characterized by an energy-momentum dispersion relation $E(k_z, k)$ given in Eq. (44). Note that k_z and k are momenta conjugate to the coordinate z and chain index y_j . Since y_j takes discrete values with its increment $2\pi l^2/L_x$, the dispersion is periodic in k with respect to the first Brillouin zone, $E(k_z, k + \frac{L_x}{l^2}) = E(k_z, k)$.

Unlike its dispersion along k_z , $E(k_z, k)$ for $L_x \gg l$ has a unique dispersion along k due to the ‘infinite-range’ nature of the interchain rigidity. Namely, the interchain rigidity ranges over the magnetic length l , within which all the $\mathcal{O}(L_x/l)$ -number of chains are *ferromagnetically* coupled with one another. Accordingly, the collective modes with $|k| \gg l^{-1}$ always feel the interchain rigidity term in an out-of-phase way, giving rise to a finite and constant mass at $k_z = 0$ (“optical mode”);

$$E(k_z, k) = \begin{cases} \sqrt{u^2 k_z^2 + \omega_J^2} & \text{for } \frac{1}{l} \ll |k| < \frac{L_x}{2l^2}, U = 0, \\ \sqrt{u^2 k_z^2 + \omega_c^2} & \text{for } \frac{1}{l} \ll |k| < \frac{L_x}{2l^2}, U \neq 0. \end{cases} \quad (48)$$

The mass is given by $\omega_J^2 = 4\pi u K J$ for incommensurate electron filling case without the umklapp term ($U = 0$) and $\omega_c^2 = 4\pi u K (J + U)$ for the commensurate electron filling case with the umklapp term ($U \neq 0$). J and U are defined in Eq. (30). Meanwhile, the collective modes with $|k| \ll l^{-1}$ show usual acoustic-phonon behaviours (“acoustic mode”);

$$E(k_z, k) = \begin{cases} \sqrt{u^2 k_z^2 + \gamma^2 k^2} & \text{for } |k| \ll \frac{1}{l}, U = 0, \\ \sqrt{u^2 k_z^2 + \gamma^2 k^2 + \omega_U^2} & \text{for } |k| \ll \frac{1}{l}, U \neq 0. \end{cases} \quad (49)$$

Note that the umklapp term endows the ‘acoustic mode’ with a finite mass at $k_z = k = 0$, $\omega_U^2 = 8\pi u K U$.

In the thermodynamic limit ($L_x \gg l$), the number of the optical modes within the first Brillouin zone becomes much larger than the acoustic modes (Fig. 6). Thereby, the integral for the self-energy part in Eq. (42) is domi-

nated by the optical-mode contribution in large L_x limit;

$$\begin{aligned}
& \frac{1}{L_z N} \sum_{\mathbf{k}} [M_0^{-1}(\mathbf{k}, \omega_n)]_{2,2} \\
&= \frac{l^2}{L_x} \int \frac{dk_z}{2\pi} \int_{-\frac{L_x}{2l^2}}^{\frac{L_x}{2l^2}} dk \frac{\pi u K}{\omega_n^2 + E^2(k_z, k)} \\
&= \begin{cases} \int \frac{dk_z}{2\pi} \frac{\pi u K}{u^2 k_z^2 + \omega_n^2 + \omega_J^2} = \frac{\pi K}{2} \frac{1}{\sqrt{\omega_n^2 + \omega_J^2}} & (U = 0), \\ \int \frac{dk_z}{2\pi} \frac{\pi u K}{u^2 k_z^2 + \omega_n^2 + \omega_c^2} = \frac{\pi K}{2} \frac{1}{\sqrt{\omega_n^2 + \omega_c^2}} & (U \neq 0). \end{cases} \quad (50)
\end{aligned}$$

Substituting Eq. (50) into eq. Eq. (42), we get $\overline{Q_{zz}(i\omega_n)}$;

$$\overline{Q_{zz}(i\omega_n)} = \frac{e^2 u K}{\pi^2 l^2} \frac{\omega_n}{\omega_n^2 + 2u\pi K U(0) - \frac{\pi^2 K^2 u g_y}{\sqrt{\omega_n^2 + \omega_*^2}}}, \quad (51)$$

where $\omega_* = \omega_J$ for incommensurate filling case ($U = 0$) and $\omega_* = \omega_c$ for commensurate filling case ($U \neq 0$). By the analytic continuation, $i\omega_n = \omega + i\eta$, we finally obtain the conductivity $\overline{\sigma_{zz}(\omega)}$ in these two cases as in eqs. (5,6) (see the following two subsections).

C. Conductivity in DW phase (incommensurate electron filling case)

For the DW phase without the umklapp term (incommensurate electron filling case; $U = 0$), the Fourier transformed imaginary-time correlation function takes a form of,

$$\overline{Q_{zz}(i\omega_n)} = \frac{e^2 u K}{\pi^2 l^2} \omega_n \left\{ \omega_n^2 - \frac{\pi^2 K^2 u g_y}{\sqrt{\omega_n^2 + \omega_J^2}} \right\}^{-1}. \quad (52)$$

In the clean limit ($g_y = 0$), the function has the first order pole at $\omega_n = 0$,

$$Q_{zz}(i\omega_n) = \frac{e^2 u K}{\pi^2 l^2} \frac{1}{\omega_n}. \quad (53)$$

Thus, the real part of the optical conductivity has a delta function peak at $\omega = 0$ ('Drude peak'),

$$\text{Re}\sigma_{zz}(\omega) = \frac{e^2 u K}{\pi l^2} \delta(\omega). \quad (54)$$

Once finite disorder (g_y) is introduced, the Drude peak disappears immediately. Instead, it acquires a finite continuum spectrum above a threshold frequency ω_J . The threshold frequency is the mass of the optical mode at $k_z = 0$. This situation can be seen from the conductivity, obtained by the analytic continuation of $\overline{Q_{zz}(i\omega_n)}$ in the complex ω plane ($i\omega_n \rightarrow \omega + i0$);

$$\begin{aligned}
\overline{\sigma_{zz}(\omega)} &= \frac{e^2 u K}{\pi^2 l^2} (-i)\omega \left\{ -\omega^2 - \frac{\pi^2 K^2 u g_y}{\sqrt{|\omega^2 - \omega_J^2|}} \right. \\
&\quad \times \left. [\Theta(\omega_J - |\omega|) + i\text{sgn}(\omega)\Theta(|\omega| - \omega_J)] \right\}^{-1},
\end{aligned}$$

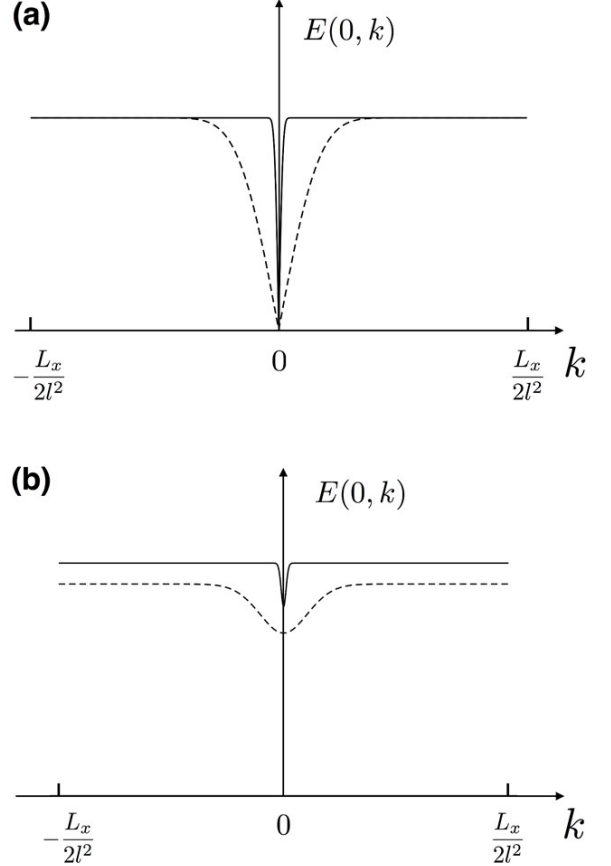


FIG. 6. (color online) Energy-momentum dispersion relation for collective mode with $k_z = 0$ for different L_x . Solid line is for $\lambda = 40$ and dashed line is for $\lambda = 4$ with $\lambda \equiv L_x/(2\pi l)$. We used Eqs. (44,46,47,25,27) for this calculation. (a) incommensurate electron filling case (without umklapp term; $U = 0$). (b) commensurate electron filling case (with umklapp term; $U \neq 0$).

or its real part,

$$\overline{\text{Re}\sigma_{zz}(\omega)} = \frac{e^2 u K}{\pi^2 l^2} \frac{\pi^2 K^2 u g_y}{\sqrt{\omega^2 - \omega_J^2}} \frac{|\omega|\Theta(|\omega| - \omega_J)}{\omega^4 + \frac{(\pi^2 K^2 u g_y)^2}{\omega^2 - \omega_J^2}}. \quad (55)$$

As is clear from this derivation, the continuum spectrum at $\omega > \omega_J$ stems from the optical modes with finite k_z . The spectrum starts with $\sqrt{\omega - \omega_J}$ near the threshold frequency ω_J and decays with ω^{-4} in high frequency side (Fig. 7(b)).

D. Conductivity in DW phase (commensurate electron filling case)

For the density wave phase with the umklapp term (commensurate electron filling case; $U \neq 0$), the optical conductivity in the clean limit ($g_y = 0$) has a resonance

peak at a finite frequency ω_U ;

$$\text{Re}\sigma_{zz}(\omega) = \frac{e^2 u K}{2\pi l^2} \delta(|\omega| - \omega_U) \quad (56)$$

where the resonance frequency $\omega_U \equiv \sqrt{8\pi u K U}$ stands for the mass of the acoustic mode at $k = k_z = 0$. Once the disorder is introduced ($g_y \neq 0$), the mass is renormalized into a smaller value ($\omega = \omega_0$). Besides, the optical conductivity acquires a continuum spectrum above the threshold frequency ω_c (Fig. 7(c)). The threshold frequency ω_c is nothing but the mass of the optical mode at $k_z = 0$ and $k \neq 0$. The disorder strength has a critical value $g_{y,c}$ at which the renormalized mass ω_0 of the acoustic mode becomes zero and above which the resonance peak disappears;

$$g_{y,c} \equiv \frac{\omega_U^2 \omega_c}{u \pi^2 K^2}.$$

These results can be obtained in the following way. Firstly, the optical conductivity is given by,

$$\overline{\sigma_{zz}(\omega)} = \frac{\omega}{F_-(\omega + i\eta)\Theta(\omega_c - |\omega|) + F_+(\omega)\Theta(|\omega| - \omega_c)}, \quad (57)$$

with

$$F_-(\omega) \equiv -\omega^2 + \omega_U^2 - \frac{\pi^2 K^2 u g_y}{\sqrt{\omega_c^2 - \omega^2}},$$

$$F_+(\omega) \equiv -\omega^2 + \omega_U^2 - i \frac{\pi^2 K^2 u g_y}{\sqrt{\omega^2 - \omega_c^2}} \text{sgn}(\omega).$$

When the disorder strength is weaker than the critical value ($g_y < g_{y,c}$), a real ω solution of $F_-(\omega) = 0$ exists with $F'_-(\omega) \neq 0$. This leads to

$$\overline{\text{Re}\sigma_{zz}(\omega)} = \frac{e^2 u K}{\pi l^2} \frac{\omega_0}{|F'_-(\omega_0)|} \delta(|\omega| - \omega_0) \Theta(\omega_c - |\omega|) + \frac{e^2 u^2 K^3 g_y}{l^2 \sqrt{\omega^2 - \omega_c^2}} \frac{|\omega| \Theta(|\omega| - \omega_c)}{(\omega^2 - \omega_U^2)^2 + \frac{(\pi^2 K^2 u g_y)^2}{(\omega^2 - \omega_c^2)}}. \quad (58)$$

The continuum above the threshold frequency is essentially of the same origin as in eq. (55). When the disorder strength is greater than the critical value ($g_y > g_{y,c}$), $F_-(\omega) = 0$ has no real-valued solution. In this case, the optical conductivity has only the continuum spectrum,

$$\overline{\text{Re}\sigma_{zz}(\omega)} = \frac{e^2 u^2 K^3 g_y}{l^2 \sqrt{\omega^2 - \omega_c^2}} \frac{|\omega| \Theta(|\omega| - \omega_c)}{(\omega^2 - \omega_U^2)^2 + \frac{(\pi^2 K^2 u g_y)^2}{(\omega^2 - \omega_c^2)}}. \quad (59)$$

E. Conductivity in normal phase (decoupled one-dimensional chains)

In the normal phase ($J = U = 0$), the system reduces to decoupled 1D Luttinger liquids. In the limit, Fukuyama already calculated essentially the same quantity in a context of conductivity in the Peierls-Frohlich state with disorders³⁷;

$$\overline{\text{Re}\sigma_{zz}(\omega)} = \frac{e^2 u K}{\pi^2 l^2} \frac{\pi^2 K^2 u g_y}{\omega^4 + \frac{(\pi^2 K^2 u g_y)^2}{\omega^2}}. \quad (60)$$

The optical conductivity reduces to zero at $\omega = 0$ with ω^2 and decays as $1/\omega^4$ in large ω region (Fig. 7(a)).

IV. SINGLE-PARTICLE SPECTRAL FUNCTION IN DENSITY WAVE PHASE

A partition function of the effective boson models in eqs. (24,26) for the DW phases can be seen as a (2+1)D XY model with/without Potts term (see eqs. (B1,B2) for the partition functions of the effective boson models),

$$Z = \begin{cases} \int D\Phi_{\mathbf{j}} \exp \left[\sum_{\mathbf{j}} \left\{ J_{\tau} \cos(\Phi_{\mathbf{j}} - \Phi_{\mathbf{j}+a_{\tau}e_{\tau}}) + J_z \cos(\Phi_{\mathbf{j}} - \Phi_{\mathbf{j}+a_z e_z}) + \sum_n J_{y,n} \cos(\Phi_{\mathbf{j}} - \Phi_{\mathbf{j}+na_y e_y}) \right\} \right] & U = 0 \\ \int D\Phi_{\mathbf{j}} \exp \left[\sum_{\mathbf{j}} \left\{ J_{\tau} \cdots + J_z \cdots + \sum_n J_{y,n} \cdots + \sum_n U_{y,n} \cos(\Phi_{\mathbf{j}} + \Phi_{\mathbf{j}+na_y e_y}) \right\} \right] & U \neq 0 \end{cases} \quad (61)$$

where \cdots parts in the second line are same as in the first line. The $U(1)$ phase degree of freedom plays role of the displacement field along the field direction (z -direction); $\Phi_{\mathbf{j}} = 2\phi_m(z, \tau)$. The three-dimensional cubic-lattice co-

ordinate $\mathbf{j} = (j_z a_z, j_y a_y, j_{\tau} a_{\tau})$ represents the spatial coordinate along the field direction (z), chain index (y_j) and imaginary time (τ) respectively; $\mathbf{j} = (z, y_j, \tau)$. The lattice constants of the cubic lattice are $a_z = u a_{\tau} = \alpha$,

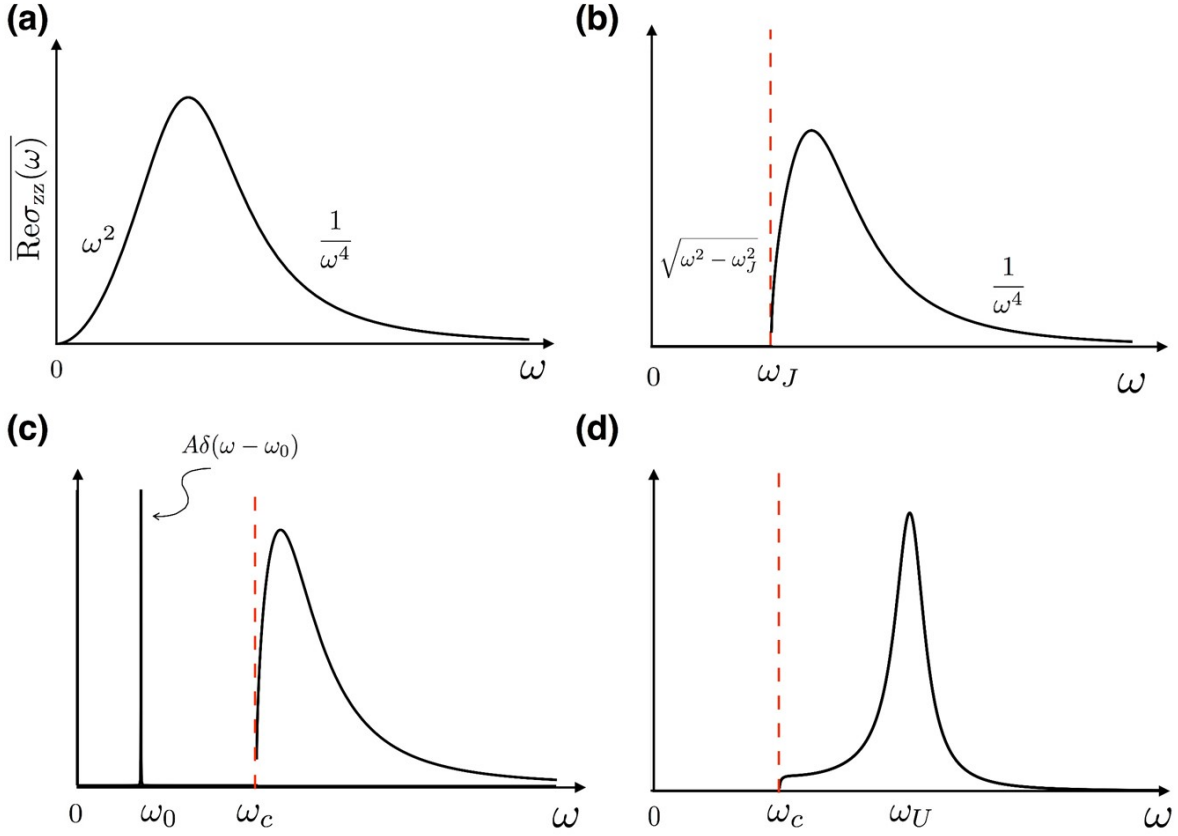


FIG. 7. (color online) Optical conductivity with disorders for different cases. (a) normal phase (decoupled one-dimensional chains)³⁷. (b) density wave phase at incommensurate electron filling case ($U = 0$). (c) density wave phase at commensurate electron filling case ($U \neq 0$) for weak disorder ($g_y \leq g_{y,c}$). (d) density wave phase at commensurate electron filling case with $\omega_U > \omega_c$.

$a_y = 2\pi l^2/L_x$. Gradient terms along the z -direction and τ -direction are regularized into a cubic lattice as the nearest neighbor coupling terms with $J_z = u^2 J_\tau = 1/(\pi K)$. The coupling along the y -direction ranges over the magnetic length;

$$J_{y,n} = \frac{\sqrt{2\pi}l}{L_x} J u \alpha^2 e^{-\frac{y_n^2}{2l^2}}, \quad U_{y,n} = \frac{\sqrt{2\pi}l}{L_x} U u \alpha^2 e^{-\frac{y_n^2}{2l^2}} \quad (62)$$

As is obvious from Eq. (61), the model at incommensurate electron filling case ($U = 0$) possesses the continuous $U(1)$ symmetry, $\Phi_j \rightarrow \Phi_j + \varphi$, that is the translational symmetry along the field direction. Meanwhile, at the commensurate electron filling case (m/n filling case with n, m mutually prime integers), the $U(1)$ symmetry reduces to the discrete Z_n symmetry due to the umklapp terms (Potts terms); $\Phi_j \rightarrow \Phi_j + \frac{2\pi}{n}$.

Breaking the continuous symmetry spontaneously, the DW phase in the incommensurate filling case has a gapless low-energy collective excitation (Fig. 6(a)), whose effect as well as disorder effect on the conductivity has been discussed in the previous section. Since the low-energy excitation is a fluctuation of charge current den-

sity and electronic displacement, we can naturally expect that such gapless low-energy excitation has also significant influence on the single-particle spectral function.

In expectation of this, we calculate in this section the spectral function in the DW phase at incommensurate electron filling case and its neighboring normal phase. For a reason which will become clear below, we consider a thin torus limit ($L_x \simeq l$) without any disorder. In this limit, the interchain rigidity ranges only over a couple of chains, so that we may begin with a ‘nearest-neighbor’ 2+1D XY model given by

$$Z_{XY} \equiv \int D\Phi_j \exp \left[\sum_{j,\mu} J \cos(\Phi_j - \Phi_{j+a_\mu e_\mu}) \right] \quad (63)$$

where the couplings along the three directions are chosen to be same, $J_\tau = J_z = J_y = J$ for simplicity. Like in the case with larger L_x , the above partition function shows a $T = 0$ quantum phase transition between the DW phase for larger J and the normal phase for smaller J ³³. The DW/normal phases for larger L_x are expected to be continuously connected to the DW/normal phases

in the thin torus limit. We thus regard that qualitative aspect of these two phases will not change on changing L_x .

A. Single-particle Matsubara Green Function

A central idea of our calculation of the spectral function in these two phases is to relate the single-particle

$$\begin{aligned} \mathcal{G}_{\sigma,j}(z_1 - z_2, \tau_1 - \tau_2) &\equiv \frac{1}{\text{Tr}[e^{-\beta\hat{\mathcal{H}}}]}\text{Tr}[e^{-\beta\hat{\mathcal{H}}}\mathcal{T}_\tau\{\psi_{H,\sigma,j}(z_1, \tau_1)\psi_{H,\sigma,j}^\dagger(z_2, \tau_2)\}] = \\ &= -\frac{\text{sgn}(\tau - \tau')}{Z_{XY}} \int_{(\Delta \cdot \mathbf{B})_{\vec{j}} = (\delta_{\vec{j}, \mathbf{N}_1} - \delta_{\vec{j}, \mathbf{N}_1 + a_y \mathbf{e}_y}) - (\delta_{\vec{j}, \mathbf{N}_2} - \delta_{\vec{j}, \mathbf{N}_2 + a_y \mathbf{e}_y})} D\Phi_j \exp \left[\sum_{j,\mu} J_\mu \cos(\Phi_j - \Phi_{j+a_\mu \mathbf{e}_\mu} + 2\pi A_{j,\mu}) \right]. \end{aligned} \quad (64)$$

Here $\hat{\mathcal{H}} \equiv \mathcal{H}_{\text{kin}} + \mathcal{H}'$ denotes the interacting electron Hamiltonian (\mathcal{H}_{kin} given by eq. (18) and \mathcal{H}' given by eq. (21) only with $j = n$ or $m = n$), $\psi_{H,\sigma,j}(z, \tau) \equiv e^{\tau\hat{\mathcal{H}}}\psi_{\sigma,j}(z)e^{-\tau\hat{\mathcal{H}}}$. $\sigma = \pm$ specifies left or right mover fermion for each chain j . The magnetic monopole lives on a dual cubic lattice site denoted by $\overline{\mathbf{N}}_{1/2}$, while the fermion's creation and annihilation operator live on a original cubic lattice site denoted by $(z_{1/2}, y_j, \tau_{1/2})$. In Eq. (64), these two coordinates are linked with each other (Fig. 8(a)),

$$(z_\mu, y_j, \tau_\mu) = \overline{\mathbf{N}}_\mu + a_y \frac{e_y}{2} + a_z \frac{e_z}{2} + a_\tau \frac{e_\tau}{2} \quad (65)$$

with $\mu = 1, 2$.

The magnetic monopole emits a quantized magnetic flux \mathbf{B} ('Dirac string'). The flux lives on a link of the dual cubic lattice, penetrating through a center point of a plaquette of the original cubic lattice. An associated gauge field \mathbf{A} lives on a link of the original lattice,

penetrating through a center of a plaquette of the dual cubic lattice. The gauge field is coupled with the U(1) phase of the XY model as in eq. (64). Accordingly, single monopole at $\overline{\mathbf{N}}_1$ creates a branchcut for the U(1) phase Φ_j in a region of $\tau > \tau_1 - a_\tau/2$, $z = z_1 - a_z/2$ and $y < y_j - a_y/2$ (Fig. 8(b)). On crossing the branchcut from $z < z_1 - a_z/2$ to $z > z_1 - a_z/2$, Φ_j acquires -2π phase winding. Meanwhile, single antimonopole at $\overline{\mathbf{N}}_1 + a_y \mathbf{e}_y$ creates a branchcut in a region of $\tau > \tau_1 - a_\tau/2$, $z = z_1 - a_z/2$ and $y < y_j + a_y/2$, on crossing which from $z < z_1 - a_z/2$ to $z > z_1 - a_z/2$, Φ_j acquires a $+2\pi$ phase winding. Therefore, a pair of the monopole and antimonopole inserted at $\overline{\mathbf{N}}_1$ and $\overline{\mathbf{N}}_1 + a_y \mathbf{e}_y$ respectively creates a branchcut in a region of $\tau > \tau_1 - a_\tau/2$, $z = z_1 - a_z/2$ and $y_j - a_y/2 < y < y_j + a_y/2$, on crossing which from $z < z_1 - a_z/2$ to $z > z_1 - a_z/2$ the phase acquires $+2\pi$ phase winding (Fig. 8(c)). Now that $\Phi_j = 2\phi_j(z, \tau)$ and $\partial_z \phi_j(z, \tau) = -\pi \rho_j(z, \tau)$, the branchcut is nothing but an addition of one hole at $z = z_1$, $y = y_j$ and $\tau \geq \tau_1$. Or equivalently, an insertion of annihilation operator $\psi_{\sigma,j}(z_1)$ at $\tau = \tau_1$;

$$\begin{aligned} &\frac{1}{\text{Tr}[e^{-\beta\hat{\mathcal{H}}}]}\text{Tr}[e^{-\beta\hat{\mathcal{H}}}\mathcal{T}_\tau\{\psi_{H,\sigma,j}(z_1, \tau_1) \cdots \}] = \\ &= -\frac{\text{sgn}(\tau - \tau')}{Z_{XY}} \int_{(\Delta \cdot \mathbf{B})_{\vec{j}} = (\delta_{\vec{j}, \mathbf{N}_1} - \delta_{\vec{j}, \mathbf{N}_1 + a_y \mathbf{e}_y}) + \cdots} D\Phi_j \exp \left[\sum_{j,\mu} J_\mu \cos(\Phi_j - \Phi_{j+a_\mu \mathbf{e}_\mu} + 2\pi A_{j,\mu}) \right], \end{aligned} \quad (66)$$

with $(z_1, y_j, \tau_1) = \overline{\mathbf{N}}_1 + a_y \mathbf{e}_y/2 + a_z \mathbf{e}_z/2 + a_\tau \mathbf{e}_\tau/2$. Note that the above identification of the magnetic dipole with the annihilation operator does not depend on a specific choice of the branchcut. For example, we can also re-

gard that the dipole creates a branchcut in a region of $\tau < \tau_1 - a_\tau/2$, $z = z_1 - a_z/2$ and $y_j - a_y/2 < y < y_j + a_y/2$, on crossing which from $z < z_1 - a_z/2$ to $z > z_1 - a_z/2$ the phase acquires -2π phase winding, instead of $+2\pi$

(Fig. 8(d)). Such a branchcut corresponds to an addition of particle at $z = z_1$, $y = y_j$ and $\tau \leq \tau_1$, which is again equivalent to an insertion of an annihilation operator $\psi_{\sigma,j}(z_1)$ at $\tau = \tau_1$. As is obvious from the argument, flipping the magnetic dipole exchanges annihilation operator into creation operator. This leads to eq. (64). Remark that the extra sign function $\text{sgn}(\tau_1 - \tau_2)$ in eq. (64) stems from the fermion's time ordering in the left hand side of the same equation (\mathcal{T}_τ). This maintains a proper boundary condition for the Matsubara Green function along the imaginary time axis;

$$\text{sgn}(\tau) \equiv \begin{cases} 1 & (0 < \tau < \beta), \\ -1 & (-\beta < \tau < 0). \end{cases} \quad (67)$$

B. Duality mapping to Frozen Lattice Superconductor model

By the duality transformation^{31–33}, the 3D XY model is mapped into the so-called frozen lattice superconductor model (FLS), where a U(1) phase of the superconducting order parameter $\theta_{\vec{j}}$ is coupled with an internal magnetic

gauge field $\mathbf{a}_{\vec{j}}$;

$$Z_{\text{XY}} \Longleftrightarrow Z_{\text{FLS}},$$

$$Z_{\text{XY}} \equiv \int D\Phi_j \exp \left[J \sum_{\vec{j}, \mu=x, y, z, \tau} \cos \left(\Phi_j - \Phi_{j+a_\mu \mathbf{e}_\mu} \right) \right],$$

$$Z_{\text{FLS}} \equiv \lim_{t \rightarrow 0} \int D\mathbf{a}_{\vec{j}} D\theta_{\vec{j}} \exp \left[-S_{\text{FLS}}[\mathbf{a}_{\vec{j}}, \theta_{\vec{j}}] \right], \quad (68)$$

$$S_{\text{FLS}}[\mathbf{a}_{\vec{j}}, \theta_{\vec{j}}] \equiv \frac{1}{2J} \sum_{\vec{j}, \mu} (\nabla \times \mathbf{a})_{\vec{j}, \mu}^2 - \frac{1}{t} \sum_{\vec{j}, \mu} \cos \left(\theta_{\vec{j}} - \theta_{\vec{j}+a_\mu \mathbf{e}_\mu} - 2\pi \mathbf{a}_{\vec{j}, \mu} \right). \quad (69)$$

The U(1) phase lives on the dual cubic lattice site denoted by \vec{j} , while three components of the gauge field $\mathbf{a}_{\vec{j}} \equiv (a_{\vec{j},z}, a_{\vec{j},y}, a_{\vec{j},x})$ live on a link of the dual cubic lattice. The parameter t plays role of the temperature in the FLS model, and is taken to zero or sufficiently small (the model is referred to as ‘frozen’ lattice superconductor model). In the FLS model, smaller J suppresses spatial and temporal fluctuations of the magnetic gauge field, so that the superconducting (SC) order sets in at low temperature t ; $\langle e^{i\theta_{\vec{j}}} \rangle \neq 0$. The SC phase (‘Meissner phase’) in the FLS model corresponds to the normal phase in the XY model. In the SC phase, the gauge fields are expelled from the SC bulk. An effective theory for such phase may be crudely described by a simple omission of the magnetic gauge fields from the FLS model;

$$S_{\text{FLS}}[\mathbf{a}_{\vec{j}}, \theta_{\vec{j}}] \simeq -\frac{1}{2t} \sum_{\vec{j}, \mu} (\Delta_\mu \theta_{\vec{j}})^2. \quad (70)$$

For larger J , the fluctuations of the magnetic gauge fields become wild enough that the SC order is killed by the gauge fields, $\langle e^{i\theta_{\vec{j}}} \rangle = 0$. This phase corresponds to the DW phase in the XY model. An effective theory for such non-superconducting phase in the FLS model is given only by the Maxwell term (‘Maxwell phase’):

$$S_{\text{FLS}}[\mathbf{a}_{\vec{j}}, \theta_{\vec{j}}] \simeq -\frac{1}{2J} \sum_{\vec{j}, \mu} (\nabla \times \mathbf{a})_{\vec{j}, \mu}^2. \quad (71)$$

By the duality transformation³³, the partition function of the XY model in the presence of a magnetic monopole and anti-monopole is mapped into a correlation function in the frozen lattice superconductor model,

$$\begin{aligned} & \frac{1}{Z_{\text{XY}}} \int_{(\Delta \cdot \mathbf{B})_{\vec{j}} = \pm \delta_{\vec{j}, \vec{N}} + \dots} D\Phi_j \exp \left[J \sum_{\vec{j}, \mu} \cos \left(\Phi_j - \Phi_{j+a_\mu \mathbf{e}_\mu} + 2\pi A_{j,\mu} \right) \right] \\ & \Longleftrightarrow \frac{1}{Z_{\text{FLS}}} \int D\mathbf{a}_{\vec{j}} D\theta_{\vec{j}} \exp \left[\pm i\theta_{\vec{N}} + \dots \right] \exp \left[-\frac{1}{2J} \sum (\nabla \times \mathbf{a})^2 + \frac{1}{t} \sum \cos \left(\Delta_\mu \theta_{\vec{j}} - 2\pi \mathbf{a}_{\vec{j}, \mu} \right) \right] \equiv \langle e^{\pm i\theta_{\vec{N}}} \dots \rangle_{\text{FLS}} \end{aligned} \quad (72)$$

Combined with Eq. (64), this leads to

$$\begin{aligned} & \mathcal{G}_{\sigma,j}(z_1 - z_2, \tau_1 - \tau_2) = \\ & - \text{sgn}(\tau - \tau') \langle e^{-i\theta_{\vec{N}_1} + i\theta_{\vec{N}_1 + a_y \mathbf{e}_y} + i\theta_{\vec{N}_2} - i\theta_{\vec{N}_2 + a_y \mathbf{e}_y}} \rangle_{\text{FLS}} \end{aligned} \quad (73)$$

with eq. (65).

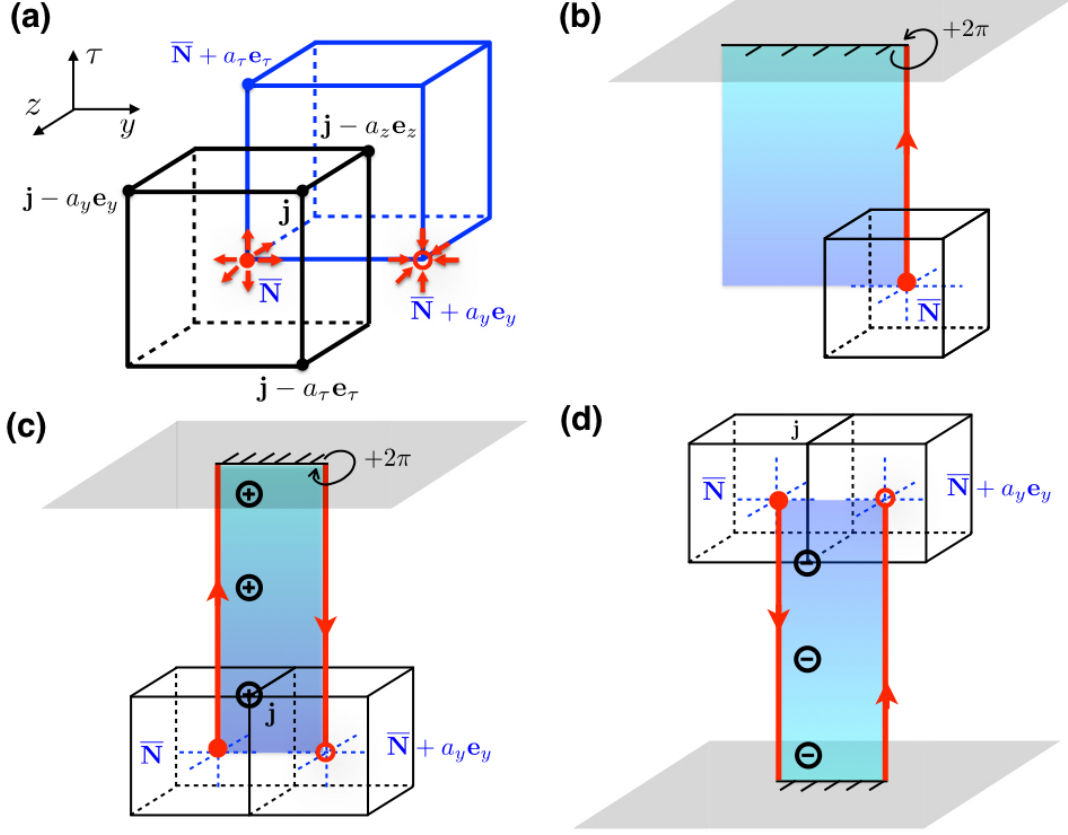


FIG. 8. (color online) (a) original cubic lattice (black) and dual cubic lattice (blue) (b) The magnetic monopole lives on a dual cubic lattice site and emits a quantized Dirac string or magnetic flux (red line with arrow). (c,d) A pair of magnetic monopole and antimonopole creates a branchcut, on crossing which from the negative z side to the positive z side the $U(1)$ phase acquires $\pm 2\pi$ respectively.

C. single-particle spectral function

Based on these foundations, we calculate the four-point correlation function of the FLS model in the SC/non-SC phase, using their respective effective theories as in eqs. (70,71). We then take a Fourier transform of the calculated four-point correlation function;

$$\mathcal{G}_{\sigma,j}(z_1 - z_2, \tau_1 - \tau_2) \equiv \frac{1}{\beta L_z} \sum_{q_z, i\omega_n} e^{iq_z(z_1 - z_2) - i\mathcal{E}_n(\tau_1 - \tau_2)} \mathcal{G}_{\sigma,j}(q_z, i\mathcal{E}_n), \quad (74)$$

with fermionic Matsubara frequency $\mathcal{E}_n = (2n + 1)\pi/\beta$. Here q_z in eq. (74) is a momentum k_z measured from σk_F with $\sigma = \pm$ and is much smaller than a_z^{-1} ; $q_z = k_z - \sigma k_F$. After an analytic continuation of $\mathcal{G}_{\sigma,j}(q_z, i\mathcal{E}_n)$ in the complex ω plane ($i\mathcal{E}_n \rightarrow \omega \pm i\delta$), we obtain the spectral function from,

$$\rho_\sigma(q_z, \omega) \equiv i \left\{ \mathcal{G}_{\sigma,j}(q_z, i\mathcal{E}_n = \omega + i\delta) - \mathcal{G}_{\sigma,j}(q_z, i\mathcal{E}_n = \omega - i\delta) \right\}. \quad (75)$$

The spectral function in the normal phase (which is calculated from the four-point correlation function of the

FLS model in the SC phase) takes a form of

$$\rho_\sigma(q_z, \omega) = 2\pi t e^{-C} \sqrt{\omega^2 - u^2 q_z^2} \Theta(|\omega| - u|q_z|) + \dots, \quad (76)$$

(see Appendix D1 for its detailed derivation). The spectral function in the DW phase (calculated from the correlation function in the non-SC phase) is given by

$$\rho_\sigma(q_z, \omega) = \frac{16\pi^3 J}{\sqrt{\omega^2 - u^2 q_z^2}} \Theta(|\omega| - u|q_z|) + \dots, \quad (77)$$

(see Appendix D2 for its derivation). Note that we omit the chain index j in the left hand sides in eqs. (75,76,77) because the calculated four-point correlation functions are independent from the chain coordinate y_j . Note also that the spectral function thus obtained gives the real and imaginary part of the real-time time-ordered Green function;

$$G_\sigma(q_z, \omega) = \mathcal{P} \int_{-\infty}^{\infty} \frac{d\omega'}{2\pi} \frac{\rho_\sigma(q_z, \omega')}{\omega - \omega'} - i\pi \tanh\left(\frac{\beta\omega}{2}\right) \rho_\sigma(q_z, \omega), \quad (78)$$

where the real-time Green function is defined as

$$iG_\sigma(z_1, t_1; z_2, t_2) \equiv \frac{1}{Z} \text{Tr} \left[\mathcal{T}_t \{ \psi_{H,\sigma,j}(z_1, t_1) \psi_{H,\sigma,j}^\dagger(z_2, t_2) \} \right],$$

$$G_\sigma(q_z, \omega) \equiv \int dt \int dz e^{-iq_z(z_1 - z_2) + i\omega(t_1 - t_2)} \times G_\sigma(z_1, t_1; z_2, t_2),$$

and $\psi_{H,\sigma,j}(z, t) \equiv e^{i\hat{\mathcal{H}}t} \psi_{\sigma,j}(z) e^{-i\hat{\mathcal{H}}t}$. $\hat{\mathcal{H}} \equiv \hat{\mathcal{H}}_{\text{kin}} + \mathcal{H}'$ with \mathcal{H}_{kin} given by eq. (18) and \mathcal{H}' given by eq. (21) only with $n = m$ or $n = j$.

V. IN-PLANE CONDUCTANCE

Unlike the out-of-plane current operator, in-plane current operators (\hat{J}_x , \hat{J}_y) are given by a creation/annihilation of the 2nd LLL electron and annihilation/creation of the LLL electrons. For the 3D isotropic metal under high magnetic field in eq. (15), they are given by

$$\hat{J}_x + i\hat{J}_y \equiv \frac{\sqrt{2}e\hbar}{m_*l} \sum_{j,k_z} c_{n=0,j,k_z}^\dagger c_{n=1,j,k_z} + \dots,$$

$$\hat{J}_x - i\hat{J}_y \equiv \frac{\sqrt{2}e\hbar}{m_*l} \sum_{j,k_z} c_{n=1,j,k_z}^\dagger c_{n=0,j,k_z} + \dots,$$

where \dots parts stand for higher LL contributions. Accordingly, when the temperature is much lower than the cyclotron frequency $\hbar\omega_0$, the in-plane transports are dominated by surface transport rather than bulk transport (at least in the clean limit). To discuss the surface transport concretely, let us choose the Landau gauge, impose the periodic boundary conditions along x , z -directions, and open boundary condition along y -direction, introduce a confining potential $V(y)$ which respects the translational symmetries along the z -direction (Fig. 4(a))³⁵,

$$\begin{cases} V(y) = 0 & \text{for } |y| < \frac{L_y}{2}, \\ V(y) > 0 & \text{for } |y| > \frac{L_y}{2}. \end{cases} \quad (79)$$

For $|y| < L_y/2$, the single-particle eigenstate for the LLL is given by eq. (17) with $n = 0$, whose eigenenergy is $\hbar^2 k_z^2 / (2m_*)$. For $|y| > L_y/2$, we may also approximately use eq. (17) as an eigenstate, provided that the confining potential $V(y)$ is slowly varying compared to the magnetic length l , $l \times |\partial_y V(y)| \ll |V(y)|$. Such a quasi-eigenstate has an energy of $\hbar^2 k_z^2 / (2m_*) + V(y_j)$ ³⁵. When changing y_j from the bulk region ($|y_j| < L_y/2$) into the edge regions ($|y_j| > L_y/2$), the two Fermi points at $k_z = \pm k_F$ in the bulk region move inward, and merge into one point at $|y_j| > L_y/2$ with $V(y_j) = \mu$ (Figs. 4(b,c)). In other words, the two parallel Fermi lines at $k_z = \pm k_F$ are connected with each other by Fermi arc states, which are localized at the two boundaries, $|y_j| > L_y/2$. Since $k_x l^2 = y_j$ in eq. (17), the Fermi arc state at $y_j > L_y/2$

carries positive k_x , and that at $y_j < -L_y/2$ carries negative k_x ; these arc states are nothing but a bundle of *chiral* Fermi edge modes^{1,36}.

When viewed along the k_z -direction, the chiral Fermi arc states are connected by Δk_z , which is smaller than $2k_F$ (Fig. 4(d)). Thus, the arc states except for their two end-point states are robust against the density wave formation in the bulk. Only the two end-point states repel each other with a help of the density wave order in the bulk, such that the Fermi arc state at $k_z = k_F$ is continuously connected with the arc state at $k_z = -k_F$ as a function of k_z (Fig. 4(d)). This leads to a perfect disconnection between the arc state at $y > L_y/2$ and that at $y < -L_y/2$.

The chiral Fermi arc states often dominate low- T in-plane transports in actual experiments. For example, a graphite sample of $50 \mu\text{m}$ thickness shows an in-plane resistance of the order of $2 \Omega \sim 4 \Omega$ above the quantum limit^{16,17}. Since an interlayer lattice constant (a_z) is on the order of 0.5nm in graphite, the sample with $50\mu\text{m}$ thickness could have $10^5 (= L_z/a_z)$ number of the k_z points within the first Brillouin zone along k_z , $[-\pi/a_z, \pi/a_z]$. Assuming that $2k_F$ is several times smaller than $2\pi/a_z$, one can expect that the number of chiral Fermi edge modes at each surface is on the order of 10^4 . Since different edge modes at the same surface do not have an electron exchange much, a bundle of chiral Fermi edge modes can be regarded as a parallel circuit. Accordingly, an in-plane resistance due to the chiral Fermi arc states can be evaluated on the order of $\hbar/e^2 \times 10^{-4} \simeq 2.5\Omega$, which is on the same order of the experimental values ($2\Omega \sim 4\Omega$).

The chiral Fermi arc state at $y_j > L_y/2$ and that at $y_j < -L_y/2$ are apparently disconnected by the DW order in the bulk. One may therefore expect that these chiral surface states provide robust in-plane conductance. Contrary to this expectation, we argue in the following that the in-plane conductance due to the surface states may have a non-trivial temperature dependence, especially when the bulk electronic state has dissipative feature as in Eqs. (76,77,78).

A. Coupling between surface and bulk states

To see this, let us begin with a simple model which includes a coupling between surface and bulk states;

$$\begin{aligned}
\mathcal{H}_t &= \mathcal{H}_b + \mathcal{H}_s + \mathcal{H}_c, \\
\mathcal{H}_s &= \sum_{k_z, j}^{|y_j| > \frac{L_y}{2}} (\epsilon_{s,j}(k_z) - \mu) d_{s,j,k_z}^\dagger d_{s,j,k_z}, \\
\mathcal{H}_b &= \sum_{k_z, j}^{|y_j| < \frac{L_y}{2}} (\epsilon_b(k_z) - \mu) d_{b,j,k_z}^\dagger d_{b,j,k_z} + \mathcal{H}', \\
\mathcal{H}_c &= \sum_{j,m}^{|y_j| > \frac{L_y}{2}, |y_m| < \frac{L_y}{2}} \{T_{j,m} d_{s,j,k_z}^\dagger d_{b,m,k_z} + \text{h.c.}\}.
\end{aligned} \tag{80}$$

Here $\epsilon_b(k_z) \equiv \hbar^2 k_z^2 / (2m_*)$ and $\epsilon_{s,j}(k_z) \equiv \hbar^2 k_z^2 / (2m_*) + V(y_j)$ are single-particle energies of bulk and surface states with k_z and j respectively. The single-particle states for d_{s,j,k_z}^\dagger and d_{b,j,k_z}^\dagger are all in the LLL and their wavefunctions are given by eq. (17) with $n = 0$;

$$\begin{cases} d_{s,j,k_z} = c_{n=0,j,k_z} & |y_j| > \frac{L_y}{2}, \\ d_{b,j,k_z} = c_{n=0,j,k_z} & |y_j| < \frac{L_y}{2}. \end{cases} \tag{81}$$

\mathcal{H}' denotes the interaction part among electrons in the bulk states. We assume that electrons in the surface states are non-interacting. A finite spatial gradient of the confining potential ($|\partial_y V(y)|$) together with small roughness along the x -direction induces a mixing between $c_{n=0,j,k_z}$ and $c_{n=0,m,k_z}$ with $j \neq m$. This leads to a finite single-particle coupling between the surface and bulk states as in \mathcal{H}_c . For simplicity, we assume that the coupling preserves the momentum k_z .

To see the effect of this surface-bulk coupling, let us introduce real-time time-ordered Green functions for surface and bulk states;

$$G_{\mu\nu}(j, t; m, t'; k_z) \equiv \frac{1}{Z_t} \text{Tr} \left[e^{-\beta \mathcal{H}_t} \mathcal{T}_t \{ d_{\mu,j,k_z}(t) d_{\nu,m,k_z}^\dagger(t') \} \right],$$

with $\mu, \nu = s, b$ and $d_{\mu,j,k_z}(t) \equiv e^{i\mathcal{H}_t t} d_{\mu,j,k_z} e^{-i\mathcal{H}_t t}$. According to Eq. (80), equation of motions (EOMs) for these Green functions are given by,

$$\begin{aligned}
&(-i\partial_t + (\epsilon_{s,j}(k_z) - \mu)) G_{ss}(j, t; j, t'; k_z) = -\delta(t - t') \\
&\quad - \sum_m^{|y_m| < \frac{L_y}{2}} T_{j,m} G_{bs}(m, t; j, t'; k_z), \\
&(-i\partial_t + (\epsilon_{s,j}(k_z) - \mu)) G_{bs}(m, t; j, t'; k_z) \\
&\quad = - \sum_n^{|y_n| < \frac{L_y}{2}} T_{j,n}^* G_{bb}(m, t; n, t'; k_z). \tag{82}
\end{aligned}$$

The coupled EOMs can be further solved in favor for the

surface Green function,

$$\begin{aligned}
iG_{ss}(j, j; k_z, \omega) &= \int_{-\infty}^{\infty} ds e^{i\omega s} iG_{ss}(j, t+s, j, t; k_z) \\
&= \frac{i}{\omega - (\epsilon_{s,j}(k_z) - \mu)} \left\{ 1 - \frac{i}{\omega - (\epsilon_{s,j}(k_z) - \mu)} \right. \\
&\quad \times \sum_{n,m}^{|y_n|, |y_m| < \frac{L_y}{2}} T_{j,n} T_{m,j}^* iG_{bb}(n, m; k_z, \omega) \Big\}. \tag{83}
\end{aligned}$$

When the surface-bulk coupling $T_{j,m}$ is small enough, the bulk Green function $G_{bb}(n, m; k_z, \omega)$ in the right hand side could be replaced by the Green function determined *only* by the bulk Hamiltonian \mathcal{H}_b . Such a Green function is diagonal in n and m , because \mathcal{H}_b respects the translational symmetry along the x -direction;

$$G_{bb}(j, t; m, t'; k_z) = G_{bb}^0(j, t; j, t'; k_z) \delta_{j,m} + \mathcal{O}(T^2). \tag{84}$$

When k_z is proximate to the two Fermi points, $k_z \simeq \pm k_F$, $G_{bb}^0(j, t; j, t'; k_z)$ in the right hand side or its Fourier transform can be further replaced by eqs. (78,76) or by eqs. (78,77);

$$\begin{aligned}
G_{bb}^0(j, j; \omega, k_z) &= \int_{-\infty}^{\infty} ds e^{i\omega s} iG_{bb}^0(j, t+s; j, t; k_z), \tag{85} \\
&= \begin{cases} G_+(k_z - k_F, \omega) & \text{for } k_z \simeq k_F, \\ G_-(k_z + k_F, \omega) & \text{for } k_z \simeq -k_F. \end{cases} \tag{86}
\end{aligned}$$

On the one hand, Eq. (83) can be rewritten in the following way up to the second order in $T_{j,m}$;

$$\begin{aligned}
G_{ss}(j, j; k_z, \omega) &= \\
&= \frac{1}{\omega - (\epsilon_{s,j}(k_z) - \mu) - \sum_m |T_{j,m}|^2 G_{bb}^0(m, m; k_z, \omega)} + \mathcal{O}(T^4) \tag{87}
\end{aligned}$$

Eq. (87) together with Eqs. (86,78,76,77) dictates that *all* the chiral surface arc states within the following energy-momentum region ('dissipative region');

$$|\omega| > u|k_z - \sigma k_F| \tag{88}$$

($\sigma = \pm$) acquire a finite life time due to the bulk-surface coupling and the dissipative nature of the bulk electronic states in the same region. More generally, the region can be seen as the low-energy limit of the following momentum-energy region by,

$$|\omega| > \left| \frac{\hbar^2 k_z^2}{2m_*} - \mu \right| \tag{89}$$

(Fig. 3(b) or Fig. 5). Those chiral surface states outside the dissipative region have an infinite life time at least within our model for the bulk-surface coupling.

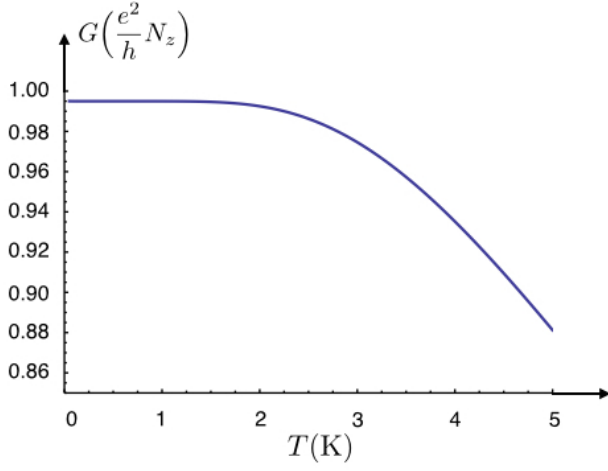


FIG. 9. (color online) Temperature dependence of the in-plane surface conductance. We choose $\epsilon_b(k_z) = \hbar^2 k_z^2 / (2m_*)$ with $m_* = m_e/18$ and $\mu = 0.355$ meV.

B. Temperature dependence of in-plane conductance

All the chiral fermi surface states *on* the Fermi level are outside the dissipative region (Fig. 5). Having an infinite life time, they give 100 % transmission for the in-plane conductance. Thus, the surface conductance at $T = 0$ is naturally quantized to be $G_s = N_z e^2 / h$ (N_z is the number of chiral edge modes within each surface). When temperature increases, the surface states within the dissipative region are thermally activated. Since they have a finite life time, the surface conductance may decrease at finite temperature.

To show this crude idea explicitly, we employ the Landauer formula³⁸ for the surface conductance;

$$G_s = \frac{e^2}{h L_x} \sum_{j, k_z} T_{j, k_z} \left(- \frac{\partial f}{\partial \epsilon} \right)_{|\epsilon = \epsilon_{s, j}(k_z)}.$$

The summation over chain index j ($y_j \equiv \frac{2\pi l^2}{L_x} j$) ranges over a half of the system including one boundary,

$$0 < y_j < y_{j, \max}$$

with $y_{j, \max} \gg \frac{L_y}{2}$. The summation over k_z ranges over the first Brillouin zone of the DW phase; $-k_F < k_z < k_F$. For simplicity, we assume that the transmission coefficient of the chiral surface state is zero in the dissipative region, while it is in-plane group velocity otherwise;

$$T_{j, k_z} = \begin{cases} 0 & \text{for } \epsilon_{s, j}(k_z) > |\epsilon_b(k_z) - \mu| \\ \frac{\partial \epsilon_{s, j}(k_z)}{\partial k_x} & \text{for } \epsilon_{s, j}(k_z) < |\epsilon_b(k_z) - \mu| \end{cases} \quad (90)$$

Here $\epsilon_{s, j}(k_z) = \hbar^2 k_z^2 / (2m_*) + V(y_j)$ and $y_j \equiv k_x l^2$. With this simplification, the surface conductance can be evaluated as

$$G_s = \frac{e^2}{h} \sum_{k_z} \left(1 - \frac{1}{e^{\beta |\epsilon_b(k_z) - \mu|} + 1} \right) \quad (91)$$

irrespective of a specific form of the confining potential $V(y)$. At the zero temperature, G_s takes the quantized value ($N_z e^2 / h$). At finite temperature, G_s decreases monotonically on increasing the temperature (Fig. 9).

VI. CONCLUSION AND OUTLOOK

In this paper, we develop a theory of transport properties of DW phases in 3D metal/semimetal under high magnetic field, which break the translational symmetries along the field direction. Such DW phases have low-energy collective excitations (phason excitations). Being comprised of fluctuations of electronic displacement (and current) along the field direction, the low-energy collective excitations have significant impacts on the longitudinal (optical) conductivity along the field direction. In section III, we calculate the conductivity in the presence of backward scattering type disorders and observe that this is indeed the case. With an addition of further theoretical studies, the calculated optical conductivities may provide better qualitative understandings of non-linear I-V characteristics of the DW phases along the field direction.

Note also that both Gaussian and Born approximations used in sec. III become invalid, when the disorders kill the DW phase itself. Especially, the single-particle backward scattering disorder introduced in eq. (36) plays role of “random magnetic field” in the XY model, while the Imry-Ma’s argument^{39–41} dictates that an infinitesimally small random magnetic field kills the ordered phase of the XY model completely^{39–41}. Thereby, the DW phase at incommensurate electron filling will be likely killed even by an infinitesimally small single-particle backward scattering type disorder. This is the case especially when the inter-chain rigidity term range only over a couple of chains. In the thermodynamic limit, the inter-chain rigidity ranges over magnetic length, within which an extensive number of chains are ferromagnetically coupled with one another (see Eqs. (25) or Eq. (62)). An Imry-Ma’s correlation function analysis suggests that, even in the presence of such a longer range interchain coupling, the incommensurate DW phase still *cannot* survive under the small disorder, unless one assume a rather awkward geometry of the system: $l L_x \geq L_z L_y$. This observation suggests us to reconsider the identities of two low-temperature resistive phases discovered by transport experiments in graphite in the quasi-quantum limit.

In section IV, we formulate a method of calculating the single-particle electron spectral function in DW and normal phases and observe that the phason excitation also changes low-energy feature of the spectral function: giving rise to an additional low-energy continuum spectra in the spectral function. In the presence of a surface-bulk coupling, the obtained spectral weight in the bulk electronic states can be transferred to the spectral functions of the chiral surface Fermi arc states, giving the latter states finite life times. Based on a simple model, we ar-

gue that this can result in a temperature-dependent in-plane surface conductance (conductance perpendicular to the magnetic field direction, carried by the chiral surface states). The obtained result may provide possible explanations for a recent in-plane transport measurements in graphite¹⁶.

ACKNOWLEDGMENTS

This work was supported by NBRP of China (Grant No. 2014CB920900 and Grant No. 2015CB921104).

Appendix A: Interacting electron Hamiltonian and its bosonization

Electronic Hamiltonian for a Weyl semimetal under high magnetic field

As another possible application of our effective boson model and analyses, we may also consider a 3D semimetal with two degenerate Weyl nodes at $\mathbf{k} = \mathbf{K}_+$ and $\mathbf{k} = \mathbf{K}_-$, having linear energy dispersion. The kinetic energy part under the magnetic field is given by

$$\mathcal{H}_{\text{kin}} = \sum_{\sigma=\pm} \int d\mathbf{r} \begin{pmatrix} \Psi_{\sigma,1}^\dagger(\mathbf{r}) & \Psi_{\sigma,2}^\dagger(\mathbf{r}) \end{pmatrix} \sigma v_F \hat{\tau} \cdot \boldsymbol{\pi} \begin{pmatrix} \Psi_{\sigma,1}(\mathbf{r}) \\ \Psi_{\sigma,2}(\mathbf{r}) \end{pmatrix}, \quad (\text{A1})$$

where $\Psi_{\sigma,\mu}(\mathbf{r})$ stands for a slowly-varying part of two-component field operators ($\mu = 1, 2$) at a Weyl node of $\mathbf{k} = \mathbf{K}_\sigma$ ($\sigma = \pm$). Namely, the electron creation operator $\Psi^\dagger(\mathbf{r})$ is expanded in terms of Bloch wavefunctions at the Weyl nodes $\Phi_{\mathbf{K}_\sigma,\mu}(\mathbf{r})$ as

$$\Psi^\dagger(\mathbf{r}) = \sum_{\sigma=\pm} \sum_{\mu=1,2} \Phi_{\mathbf{K}_\sigma,\mu}^*(\mathbf{r}) \Psi_{\sigma,\mu}^\dagger(\mathbf{r}) + \dots \quad (\text{A2})$$

The two-component slowly-varying fields are further expanded in terms of eigenstates of Eq. (A1). We keep only an eigenmode for the lowest Landau level;

$$\begin{pmatrix} \Psi_{\sigma,1}(\mathbf{r}) \\ \Psi_{\sigma,2}(\mathbf{r}) \end{pmatrix} = \frac{1}{\sqrt{\sqrt{\pi} l L_x}} \sum_j e^{ik_x x - \frac{(y-y_j)^2}{2l^2}} \begin{pmatrix} \psi_{\sigma,j}(z) \\ 0 \end{pmatrix} \quad (\text{A3})$$

with the same definitions for $j = 1, 2, \dots, L_x L_y / (2\pi l^2)$, the momentum along the x -direction $k_x \equiv 2\pi j / L_x$ and $y_j \equiv 2\pi l^2 j / L_x$. l denotes the magnetic length. We assume again that the cyclotron frequency is much higher than the cutoff energy scale associated with the kinetic energy along the z -direction, to omit the higher Landau level terms. This leads to the kinetic energy part given only by the slowly varying field operator for the LLL electrons, i.e. $\psi_{\sigma,j}(z)$. The kinetic energy part thus obtained takes the exact same form as in eq. (18). In principle, the interaction part for the Weyl semimetal should be derived

by a substitution of Eqs.(A2,A3) into Eq. (20). Depending on a form of the interaction potential $V(\mathbf{r})$ and Bloch wavefunctions at the nodes, this may not necessarily lead to a similar form as in Eq. (21). For simplicity, we assume the same interaction part as in Eq. (21) for the Weyl semimetal case.

Bosonization of the interacting electron Hamiltonian

The electron creation operator for each j is bosonized in terms of the two conjugate phase variables³⁴,

$$\psi_{\sigma,j}(z) = \frac{\eta_{\sigma,j}}{\sqrt{2\pi\alpha}} e^{-i(\sigma\phi_j(z) - \theta_j(z))} \quad (\text{A4})$$

where $\eta_{\sigma,j}$ is a Klein factor satisfying the anti-commutation relation $\{\eta_{\sigma,j}, \eta_{\sigma',m}\} = \delta_{\sigma\sigma'} \delta_{jm}$. α is a short-range cutoff for the spatial coordinate z . The two phase variables are conjugate to each other, satisfying $[\phi_j(z'), \partial_z \theta_m(z)] = i\pi \delta(z - z') \delta_{j,m}$. $\phi_j(z)$ is the displacement field along the field direction (z); spatial derivative of $\phi_j(z)$ with respect to z is the electron density,

$$\pi \rho_j(z) = -\partial_z \phi_j(z). \quad (\text{A5})$$

Besides, the momentum conjugate to the displacement field is the current density along the field,

$$\pi \Pi_j(z) = \partial_z \theta_j(z). \quad (\text{A6})$$

In terms of these phase variables, the kinetic energy part (eq.(18)) is given by;

$$H_{\text{kin}} = \sum_j \int dz \frac{v_F}{2\pi} \left\{ (\pi \Pi_j(z))^2 + (\partial_z \phi_j(z))^2 \right\}. \quad (\text{A7})$$

Due to the Klein factor (Majorana fermions), the interaction part can not be fully bosonized. Those terms in eq. (21) with $n \neq m$ and $n \neq j$ are accompanied with products of four distinct Majorana fermions. It is generally impossible to bosonize simultaneously all such terms. On the one hand, a previous parquet equation study by Yakovenko clarified that the short-range repulsive interaction such as in eq. (23) leads to a density wave order which breaks the translational symmetry along the field direction^{3,26,27}. An order parameter of such DW order is given by a particle-hole pairing within the same in-plane momentum $\langle \psi_{+,j}^\dagger(z) \psi_{-,j}(z) \rangle$. Such DW orders are primarily induced by those interactions terms in eq. (21) with $n = m$ (Fock term) or $n = j$ (Hartree term), while the others play the secondary role. To obtain an effective boson theory for the density wave order phase, we thus keep only these Hartree and Fock terms (random phase approximation). This approximation leads to a following bosonized effective Hamiltonian;

$$H_{\text{inc}} = \sum_j \int dz \left\{ \frac{uK\pi}{2} \Pi_j^2(z) + \frac{u}{2\pi K} (\partial_z \phi_j(z))^2 - \sum_{j \neq m} J_{j-m} \sigma_j^z \sigma_m^z \cos 2[\phi_j(z) - \phi_m(z)] \right\}, \quad (\text{A8})$$

for the incommensurate electron filling case and

$$H_{\text{half}} = H_{\text{inc}} - \sum_{j \neq m} \int dz U_{j-m} \sigma_j^z \sigma_m^z \cos 2[\phi_j(z) + \phi_m(z)], \quad (\text{A9})$$

for the half electron filling case. Here, the Ising variable σ_j^z is defined by two Klein factors at each chain j , $\sigma_j^z \equiv i\eta_{+,j}\eta_{-,j} = \pm 1$. To see how Eqs. (A8,A9) are derived, let us investigate the Hartree and Fock terms in the following two subsections.

Hartree term

The interaction part with $j = n$ is given by,

$$\begin{aligned} H_H &= \frac{g}{L_x} \int dz \int dz' \sum_{m,j} V_{j-m,0}(z-z') \\ &\quad \times \psi_j^\dagger(z) \psi_m^\dagger(z') \psi_m(z') \psi_j(z) \\ &= \frac{g}{L_x} \int dz \int dz' \sum_{m,j} V_{j-m,0}(z-z') \\ &\quad \times \left\{ (\rho_{+,j}(z) + \rho_{-,j}(z)) (\rho_{+,m}(z') + \rho_{-,m}(z')) \right. \\ &\quad + e^{-2ik_F(z-z')} \psi_{+,j}^\dagger(z) \psi_{-,m}^\dagger(z') \psi_{+,m}(z') \psi_{-,j}(z) \\ &\quad + e^{2ik_F(z-z')} \psi_{-,j}^\dagger(z) \psi_{+,m}^\dagger(z') \psi_{-,m}(z') \psi_{+,j}(z) \\ &\quad + e^{-2ik_F(z+z')} \psi_{+,j}^\dagger(z) \psi_{+,m}^\dagger(z') \psi_{-,m}(z') \psi_{-,j}(z) \\ &\quad \left. + e^{2ik_F(z+z')} \psi_{-,j}^\dagger(z) \psi_{-,m}^\dagger(z') \psi_{+,m}(z') \psi_{+,j}(z) \right\}, \end{aligned}$$

where density operators are defined as

$$\rho_{\pm,j}(z) \equiv \psi_{\pm,j}^\dagger(z) \psi_{\pm,j}(z) \quad (\text{A10})$$

with $\rho_j(z) \equiv \rho_{+,j}(z) + \rho_{-,j}(z) = -(\partial_z \phi_j(z))/\pi$. Substituting Eq. (A4) into Eq. (A10), we obtain

$$\begin{aligned} H_H &= \frac{\tilde{g}}{L_x} \int dz \int dz' \sum_{m,j} V_{j-m,0}(z-z') \\ &\quad \times \left\{ 4\alpha^2 (\partial_z \phi_j(z)) (\partial_{z'} \phi_m(z')) \right. \\ &\quad + e^{-2ik_F(z-z')} \sigma_j^z \sigma_m^z e^{2i(\phi_j(z) - \phi_m(z'))} \\ &\quad + e^{2ik_F(z-z')} \sigma_j^z \sigma_m^z e^{-2i(\phi_j(z) - \phi_m(z'))} \\ &\quad - e^{-2ik_F(z+z')} \sigma_j^z \sigma_m^z e^{2i(\phi_j(z) + \phi_m(z'))} \\ &\quad \left. - e^{2ik_F(z+z')} \sigma_j^z \sigma_m^z e^{-2i(\phi_j(z) + \phi_m(z'))} \right\} \quad (\text{A11}) \end{aligned}$$

with $\sigma_j^z = i\eta_{+,j}\eta_{-,j}$ and

$$\tilde{g} \equiv g/(2\pi\alpha)^2. \quad (\text{A12})$$

Note that $V_{j-m,0}(z)$ is short-ranged in z and the associated length l_0 is typically much shorter than a length

scale of the slowly-varying phase variables $\phi_j(z)$ and $\theta_j(z)$, i.e. $l_0|\partial_z \phi_j(z)|, l_0|\partial_z \theta_j(z)| \ll 1$. As such, we further employ a gradient expansion and keep only the leading order in $l_0\partial_z \phi_j(z)$ or $l_0\partial_z \theta_j(z)$. This gives

$$\begin{aligned} H_H &= \frac{\tilde{g}}{L_x} \int dz \sum_{m,j} \bar{V}_{j-m,0} \left\{ 2\alpha^2 (\partial_z \phi_j(z)) (\partial_z \phi_m(z)) \right. \\ &\quad + e^{-2k_F^2 l_0^2} \sigma_j^z \sigma_m^z \cos [2(\phi_j(z) - \phi_m(z))] \\ &\quad \left. - \sigma_j^z \sigma_m^z \cos [2(\phi_j(z) + \phi_m(z)) - 4k_F z] \right\} \quad (\text{A13}) \end{aligned}$$

where $\int dz e^{-\frac{z^2}{2l_0^2} \pm 2ik_F z} = \sqrt{2\pi} l_0 e^{-2k_F^2 l_0^2}$ is used and

$$\bar{V}_{j-m,0} = \frac{1}{\pi\sqrt{2\pi}l'} e^{-\frac{(y_j - y_m)^2}{2(l'^2 + l_0^2)}}. \quad (\text{A14})$$

The first term in eq. (A13) gives rise to renormalizations of Luttinger parameter K and Fermi velocity u . The 2nd term takes the same form as the inter-chain rigidity term in Eq. (A8). When the spatial coordinate z is lattice regularized, $4k_F z = 2\pi n$ at the half filling, where the third term takes the same form as the umklapp term in Eq. (A9). At the incommensurate electron filling case, the umklapp term can be omitted due to a fast oscillating component $e^{-i4k_F z/34}$.

Fock term

The interaction part with $m = n$ is given by

$$\begin{aligned} H_F &= \frac{g}{L_x} \int dz \int dz' \sum_{m,j} V_{0,j-m}(z-z') \\ &\quad \times \psi_m^\dagger(z) \psi_j^\dagger(z') \psi_m(z') \psi_j(z) \\ &= \frac{g}{L_x} \int dz \int dz' \sum_{m,j} V_{0,j-m}(z-z') \\ &\quad \times \left\{ \psi_{+,m}^\dagger(z) \psi_{+,j}^\dagger(z') \psi_{+,m}(z') \psi_{+,j}(z) \right. \\ &\quad + \psi_{-,m}^\dagger(z) \psi_{-,j}^\dagger(z') \psi_{-,m}(z') \psi_{-,j}(z) \\ &\quad + e^{-2ik_F(z-z')} \psi_{+,m}^\dagger(z) \psi_{-,j}^\dagger(z') \psi_{+,m}(z') \psi_{-,j}(z) \\ &\quad + e^{2ik_F(z-z')} \psi_{-,m}^\dagger(z) \psi_{+,j}^\dagger(z') \psi_{-,m}(z') \psi_{+,j}(z) \\ &\quad + \psi_{+,m}^\dagger(z) \psi_{-,j}^\dagger(z') \psi_{-,m}(z') \psi_{+,j}(z) \\ &\quad + \psi_{-,m}^\dagger(z) \psi_{+,j}^\dagger(z') \psi_{+,m}(z') \psi_{-,j}(z) \\ &\quad + e^{-2ik_F(z+z')} \psi_{+,m}^\dagger(z) \psi_{+,j}^\dagger(z') \psi_{-,m}(z') \psi_{-,j}(z) \\ &\quad \left. + e^{2ik_F(z+z')} \psi_{-,m}^\dagger(z) \psi_{-,j}^\dagger(z') \psi_{+,m}(z') \psi_{+,j}(z) \right\}. \quad (\text{A15}) \end{aligned}$$

As above, we employ the gradient expansion and keep the leading order in small $l_0\partial_z \phi_j(z)$ or $l_0\partial_z \theta_j(z)$. This

gives

$$\begin{aligned}
H_F = & \frac{\tilde{g}}{L_x} \int dz \sum_{m,j} \bar{V}_{0,j-m} \\
& \times \left\{ - (1 + e^{-2k_F^2 l_0^2}) \alpha^2 (\partial_z \phi_j(z)) (\partial_z \phi_m(z)) \right. \\
& - (1 - e^{-2k_F^2 l_0^2}) \alpha^2 (\partial_z \theta_j(z)) (\partial_z \theta_m(z)) \\
& - \sigma_j^z \sigma_m^z \cos [2(\phi_j(z) - \phi_m(z))] \\
& \left. + \sigma_j^z \sigma_m^z \cos [2(\phi_j(z) + \phi_m(z)) - 4k_F z] \right\}, \quad (A16)
\end{aligned}$$

with

$$\bar{V}_{0,m} = \frac{1}{\pi \sqrt{2\pi} l'} e^{-\frac{y_m^2}{2l'^2}}. \quad (A17)$$

The first two terms in eq. (A16) contribute to renormalizations of the Luttinger parameter and the Fermi velocity. The 2nd term and the third term contribute to the inter-chain rigidity and the umklapp term respectively. When combined together, Eqs.(A7), (A13), (A16) lead to Eq. (A8) for the incommensurate electron filling case and Eq.(A9) for the half electron filling case respectively with

$$\begin{aligned}
J_m = & \frac{\tilde{g}}{L_x} (\bar{V}_{0,m} - e^{-2k_F^2 l_0^2} \bar{V}_{m,0}) \\
= & \frac{\tilde{g}}{L_x} \frac{1}{\pi \sqrt{2\pi} l'} \left[e^{-\frac{y_m^2}{2l'^2}} - e^{-\frac{y_m^2}{2(l'^2 + l_0^2)}} e^{-2k_F^2 l_0^2} \right], \quad (A18) \\
U_m = & \frac{\tilde{g}}{L_x} (-\bar{V}_{0,m} + \bar{V}_{m,0}) \\
= & \frac{\tilde{g}}{L_x} \frac{1}{\pi \sqrt{2\pi} l'} \left[-e^{-\frac{y_m^2}{2l'^2}} + e^{-\frac{y_m^2}{2(l'^2 + l_0^2)}} \right].
\end{aligned}$$

For repulsive interaction case ($\tilde{g} > 0$), the Fock term favors positive J_m , while the Hartree term favors negative J_m ^{8,23}. When the interaction length l_0 is replaced by the Thomas-Fermi length⁴², we can typically expect that the Fock term dominates the Hartree term due to the small factor; $e^{-2k_F^2 l_0^2} \ll 1$. In the following, we consider this case and replace J_m by its value of the Fock term,

$$J_m = \frac{\tilde{g}}{L_x} \frac{1}{\pi \sqrt{2\pi} l'} e^{-\frac{y_m^2}{2l'^2}}. \quad (A19)$$

U_m given in eq. (A18) always takes a positive value, making the phason field to be locked on $0, \pi/2, \pi, 3\pi/2, \dots$. For simplicity, we take

$$U_m = \frac{\tilde{g}}{L_x} \frac{1}{\pi \sqrt{2\pi} l'} e^{-\frac{y_m^2}{2(l'^2 + l_0^2)}}. \quad (A20)$$

Appendix B: Derivation of the RG equation and RG phase diagrams

A partition function for the bosonized Hamiltonian is given by

$$\begin{aligned}
Z = & \sum_{\{\sigma_j^z\}} \int D\phi D\Pi \exp \left[- \int_0^\beta d\tau \int dz \sum_j \right. \\
& \left\{ -i \Pi_j(z) \partial_\tau \phi_j(\tau) + \frac{uK\pi}{2} [\Pi_j(z)]^2 + \frac{u}{2\pi K} [\partial_z \phi_j(z)]^2 \right. \\
& - \sum_{m \neq j} J_{j-m} \sigma_j^z \sigma_m^z \cos [2\phi_j(z) - 2\phi_m(z)] \\
& \left. \left. - \sum_{m \neq j} U_{j-m} \sigma_j^z \sigma_m^z \cos [2\phi_j(z) + 2\phi_m(z)] \right\} \right]. \quad (B1)
\end{aligned}$$

An integration over the momentum variable $\Pi_j(z)$ leads to

$$\begin{aligned}
Z = & \sum_{\{\sigma_j^z\}} \int D\phi \exp \left[- \int_0^\beta d\tau \int dz \right. \\
& \sum_j \frac{1}{2\pi K} \left\{ [\partial_\tau \phi_j(z)]^2 + [\partial_z \phi_j(z)]^2 \right\} \\
& + \sum_{\substack{j \neq m \\ j, m}} \left\{ J_{j-m} \sigma_j^z \sigma_m^z \cos [2\phi_j(z) - 2\phi_m(z)] \right. \\
& \left. \left. + U_{j-m} \sigma_j^z \sigma_m^z \cos [2\phi_j(z) + 2\phi_m(z)] \right\} \right], \quad (B2)
\end{aligned}$$

where we put u to be 1 for simplicity. The z -dependence of the displacement field has a short-range cutoff ($\alpha = 2\pi/\Lambda$);

$$\phi_j(\mathbf{r}) = \frac{1}{\beta L_z} \sum_{i\omega_n} \sum_{|k_z| < \Lambda} e^{ik_z z - i\omega_n \tau} \phi_j(\mathbf{q}), \quad (B3)$$

with $\mathbf{r} \equiv (z, \tau)$ and $\mathbf{q} \equiv (k_z, \omega_n)$. The displacement field is decomposed into rapidly-varying mode and slowly-varying mode;

$$\begin{aligned}
\phi_j(\mathbf{r}) = & \phi_j^>(\mathbf{r}) + \phi_j^<(\mathbf{r}) \\
= & \frac{1}{\beta L_z} \sum_{i\omega_n} \sum_{\Lambda' < |k_z| < \Lambda} e^{i\mathbf{q} \cdot \mathbf{r}} \phi_j(\mathbf{q}) \\
& + \frac{1}{\beta L_z} \sum_{i\omega_n} \sum_{|k_z| < \Lambda'} e^{i\mathbf{q} \cdot \mathbf{r}} \phi_j(\mathbf{q}), \quad (B4)
\end{aligned}$$

with $\mathbf{q} \cdot \mathbf{r} \equiv k_z z - \omega_n \tau$, $\Lambda' \equiv \Lambda e^{-dl}$ and small positive dl . A further integration over the rapidly-varying mode followed by a rescaling of the z coordinate and imaginary time τ , $z \rightarrow ze^{-dl}$, $\tau \rightarrow \tau e^{-dl}$, $\beta \rightarrow \beta e^{-dl}$, gives a partition function for the slowly-varying mode. The partition function thus obtained takes essentially the same form as in eq. (B2), while the coupling constant therein such

as J_{j-m} , U_{j-m} , K and β are renormalized. As shown below, the renormalization is described by the following renormalization group equations;

$$\frac{dJ_{i-j}}{dl} = \left[2 - 2K \coth \frac{\beta\Lambda}{2}\right] J_{i-j} + C(\Lambda)K \sum_n [J_{i-n}J_{n-j} + U_{i-n}U_{n-j}], \quad (\text{B5})$$

$$\frac{dU_{i-j}}{dl} = \left[2 - 2K \coth \frac{\beta\Lambda}{2}\right] U_{i-j} + 2C(\Lambda)K \sum_n J_{i-n}U_{n-j}, \quad (\text{B6})$$

with $d\beta/dl = -\beta$. The equations will be derived in terms of a perturbative expansion with respect to the

interchain rigidity term and umklapp term. Perturbative treatments for these two are mathematically same. We first derive the equation without the umklapp term (next section). We then give a brief derivation of the equations with the umklapp term (next next section).

Incommensurate electron filling case

The partition function Eq. (B2) is expanded in the interchain rigidity term up to the second order,

$$\begin{aligned} \frac{Z}{Z_0} &= \frac{1}{Z_0} \sum_{\{\sigma_j^z\}} \int D\phi e^{-S_0[\phi]} \left\{ 1 + \frac{1}{2} \int d^2\mathbf{r} \sum_{i,j}^{i \neq j} J_{i-j} \sigma_i^z \sigma_j^z \sum_{\epsilon=\pm 1} e^{i\epsilon 2[\phi_i(\mathbf{r}) - \phi_j(\mathbf{r})]} \right. \\ &\quad + \frac{1}{8} \int d^2\mathbf{r} \int d^2\mathbf{r}' \sum_{i,j}^{i \neq j} \sum_{m,n}^{m \neq n} J_{i-j} J_{m-n} \sigma_i^z \sigma_j^z \sigma_m^z \sigma_n^z \sum_{\epsilon=\pm 1, \epsilon'=\pm 1} e^{i\epsilon 2[\phi_i(\mathbf{r}) - \phi_j(\mathbf{r})]} e^{i\epsilon' 2[\phi_m(\mathbf{r}') - \phi_n(\mathbf{r}')] } + \mathcal{O}(J^3) \Big\} \quad (\text{B7}) \\ &= \frac{1}{Z_0^<} \sum_{\{\sigma_j^z\}} \int D\phi^< e^{-S_0[\phi^<]} \exp \left[\frac{1}{2} \int d^2\mathbf{r} \sum_{i,j}^{i \neq j} J_{i-j} \sigma_i^z \sigma_j^z \sum_{\epsilon=\pm 1} e^{i\epsilon 2[\phi_i^<(\mathbf{r}) - \phi_j^<(\mathbf{r})]} \langle e^{i\epsilon 2[\phi_i^>(\mathbf{r}) - \phi_j^>(\mathbf{r})]} \rangle_> \right. \\ &\quad + \frac{1}{8} \int d^2\mathbf{r} \int d^2\mathbf{r}' \sum_{i,j}^{i \neq j} \sum_{m,n}^{m \neq n} J_{i-j} J_{m-n} \sigma_i^z \sigma_j^z \sigma_m^z \sigma_n^z \sum_{\epsilon=\pm 1, \epsilon'=\pm 1} e^{i\epsilon 2[\phi_i^<(\mathbf{r}) - \phi_j^<(\mathbf{r})]} e^{i\epsilon' 2[\phi_m^<(\mathbf{r}') - \phi_n^<(\mathbf{r}')] } \\ &\quad \left. \left(\langle e^{i\epsilon 2[\phi_i^>(\mathbf{r}) - \phi_j^>(\mathbf{r})]} e^{i\epsilon' 2[\phi_m^>(\mathbf{r}') - \phi_n^>(\mathbf{r}')] } \rangle_> - \langle e^{i\epsilon 2[\phi_i^>(\mathbf{r}) - \phi_j^>(\mathbf{r})]} \rangle_> \langle e^{i\epsilon' 2[\phi_m^>(\mathbf{r}') - \phi_n^>(\mathbf{r}')] } \rangle_> \right) \right] + \mathcal{O}(J^3). \quad (\text{B8}) \end{aligned}$$

Z_0 denotes a partition function without J_{j-m} , which can be factorized into rapidly-varying mode part and slowly-varying mode part;

$$Z_0 = \int d\phi^< e^{-S_0[\phi^<]} \cdot \int d\phi^> e^{-S_0[\phi^>]} \equiv Z_0^< \cdot Z_0^> \quad (\text{B9})$$

because

$$\begin{aligned} S_0[\phi] &= \frac{1}{2\pi K} \int_0^\beta d\tau \int dz \sum_j \left\{ [\partial_\tau \phi_j(z)]^2 + [\partial_z \phi_j(z)]^2 \right\} \\ &= \frac{1}{\beta L_z} \sum_j \sum_{\mathbf{q}} \frac{q^2}{K} \phi_j(\mathbf{q}) \phi_j(-\mathbf{q}). \quad (\text{B10}) \end{aligned}$$

From Eq. (B7) to Eq. (B8), the integration over the rapid mode has been carried out and a functional of the slow mode has been re-exponentiated up to the second order in J_{j-m} ;

$$\langle \dots \rangle_> \equiv \frac{1}{Z_0^>} \int d\phi^> \dots e^{S_0[\phi^>]}. \quad (\text{B11})$$

The first term in Eq. (B8) gives a one-loop RG correction to the interchain rigidity term, while the second term gives a two-loop correction. After the rescaling, the first term takes exactly the same form as the interchain rigidity term in eq. (B2) with renormalized coupling constant;

$$J'_{j-m} = J_{j-m} \left(\frac{\Lambda}{\Lambda'} \right)^2 \left(1 - \frac{2Kd\Lambda}{\Lambda} \coth \left(\frac{\beta\Lambda}{2} \right) \right) + \mathcal{O}(d\Lambda^2),$$

and $d\Lambda \equiv \Lambda - \Lambda'$. This leads to the one-loop RG equation

$$\frac{dJ_{j-m}}{dl} = \left[2 - 2K \coth \left(\frac{\beta\Lambda}{2} \right) \right] J_{j-m} + \mathcal{O}(J^2, d\Lambda^2). \quad (\text{B12})$$

To derive the two-loop RG equation, note first that the second term in eq. (B8) vanishes when $i \neq m, n$ and $j \neq m, n$. Finite contributions come from (i) case with either one of i and j being same as either one of m and n or (ii) case with both i and j same as m and n respectively. The

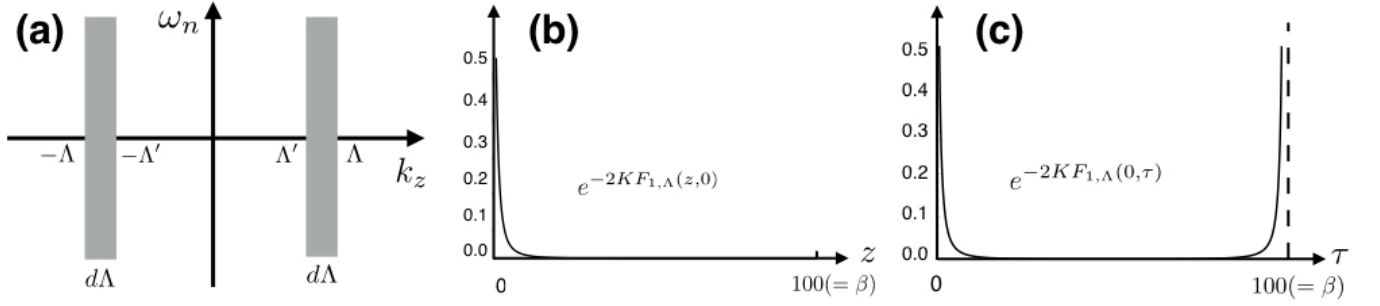


FIG. 10. (a) Schematic picture for a region of $\mathbf{q} = (k_z, i\omega_n)$ for rapidly-varying mode $\phi_j^>(\mathbf{r})$ (grey color region). $d\Lambda = \Lambda dl$ and $\Lambda' = \Lambda e^{-dl}$ (see the text). (b) $e^{-2KF_{1,\Lambda}(z,0)}$ as function of coordinate variable z . (c) $e^{-2KF_{1,\Lambda}(0,\tau)}$ as a function of the imaginary time $\tau \in [0, \beta)$. $\Lambda = 1$, $\beta = 100$, and $K = 1$.

first case generates the two-loop correction to J_{j-m} ($\epsilon\epsilon' = -1$) as well as a new cosine term $\cos(4\phi_i + 2\phi_j - 2\phi_m)$

($\epsilon\epsilon' = 1$). A scaling dimension of the new cosine term is $2 - 6K$ at $T = 0$, which is negative for $K \simeq 1$: we omit this. The case (i) with $\epsilon\epsilon' = -1$ is calculated as

$$\begin{aligned}
 (i = m, j \neq n, \epsilon\epsilon' = -1) &= \frac{1}{8} \int d^2\mathbf{r} \int d^2\mathbf{r}' \sum_{i,j,n}^{i \neq j, i \neq n} J_{i-j} J_{i-n} \sigma_j^z \sigma_n^z \sum_{\epsilon=\pm 1} e^{i\epsilon 2[\phi_i^<(\mathbf{r}) - \phi_j^<(\mathbf{r}) - \phi_i^<(\mathbf{r}') + \phi_n^<(\mathbf{r}')] } \\
 &\quad \langle e^{i\epsilon 2[\phi_i^>(\mathbf{r}) - \phi_j^>(\mathbf{r}) - \phi_i^>(\mathbf{r}') + \phi_n^>(\mathbf{r}')] } \rangle_{>} \left(1 - e^{-4\langle \phi_i^>(\mathbf{r}) \phi_i^>(\mathbf{r}') \rangle_{>}} \right) \\
 &= \frac{1}{4} \int d^2\mathbf{r} \int d^2\mathbf{r}' \sum_{i,j,n} J_{i-j} J_{i-n} \sigma_j^z \sigma_n^z : \cos(2[\phi_i^<(\mathbf{r}) - \phi_j^<(\mathbf{r}) - \phi_i^<(\mathbf{r}') + \phi_n^<(\mathbf{r}')]) : \\
 &\quad e^{-2KF_{1,\Lambda}(\mathbf{r}-\mathbf{r}')} 4dl K M_\Lambda(\mathbf{r}-\mathbf{r}') + \mathcal{O}(dl^2), \tag{B13}
 \end{aligned}$$

where

$$\begin{aligned}
 M_\Lambda(z, \tau) &\equiv \cos(\Lambda z) \{ e^{-|\tau|\Lambda} + 2 \cosh(\tau\Lambda) f_B(\Lambda) \}, \\
 e^{-2KF_{1,\Lambda}(z,\tau)} &\equiv \begin{cases} \left(\frac{B[1+(\Lambda\beta)^{-1}-iz/\beta, 1+(\Lambda\beta)^{-1}+iz/\beta]}{B[1+(\Lambda\beta)^{-1}, 1+(\Lambda\beta)^{-1}]} \right)^{2K} (1 + \Lambda^2 z^2)^{-K} & \text{for } \tau = 0, |1/\Lambda - iz| < \beta, \\ \left(\frac{B[1+(\Lambda\beta)^{-1}-\tau/\beta, 1+(\Lambda\beta)^{-1}+\tau/\beta]}{B[1+(\Lambda\beta)^{-1}, 1+(\Lambda\beta)^{-1}]} \right)^{2K} (1 + \Lambda\tau)^{-2K} & \text{for } z = 0, \end{cases} \tag{B14}
 \end{aligned}$$

with the Bose distribution function $f_B(x)$ and the Beta function $B(x, y)$. From the first line to the second line in eq. (B13), we used $\cos \phi^< =: \cos \phi^< : e^{-\frac{1}{2}\langle (\phi^<)^2 \rangle_{<}}$ and put the cosine term under the normal order denoted by “: ... :”^{34,43}. This enables the Taylor expansion within the normal order. Since $e^{-2KF_{1,\Lambda}(\mathbf{r})}$ is localized both in the z -direction and in the τ -direction (see Figs. 10(b,c)), we further employ the gradient expansion within the cosine term, to keep the leading order;

$$\begin{aligned}
 (i = m, j \neq n, \epsilon\epsilon' = -1) &= \int d^2\mathbf{r} \sum_{i,j,n} J_{i-j} J_{i-n} \sigma_j^z \sigma_n^z \\
 &\quad : \cos(2[\phi_j^<(\mathbf{r}) - \phi_n^<(\mathbf{r})]) : C(\Lambda) K dl + \mathcal{O}(\Lambda \partial_z \phi_j(z), dl^2) \tag{B15}
 \end{aligned}$$

with

$$C(\Lambda) \equiv \int d^2\mathbf{r}' e^{-2KF_{1,\Lambda}(\mathbf{r}')} M_\Lambda(\mathbf{r}'). \tag{B16}$$

This gives the two-loop RG correction to the interchain rigidity term;

$$\begin{aligned}
 J'_{j-m} &= J_{j-m} \left(1 + dl \left[2 - 2K \coth\left(\frac{\beta\Lambda}{2}\right) \right] \right) \\
 &\quad + dl C(\Lambda) K \sum_i J_{i-j} J_{i-m} + \mathcal{O}(J^3, dl^2) \tag{B17}
 \end{aligned}$$

Equivalently, we have

$$\frac{dJ_{i-j}}{dl} = \left[2 - 2K \coth\left(\frac{\beta\Lambda}{2}\right) \right] J_{i-j} + C(\Lambda) K \sum_n J_{i-n} J_{n-j} \tag{B18}$$

The second case, (ii) $i = m$ and $j = n$, generates a correction to the Luttinger parameter K ($\epsilon\epsilon' = -1$) as well as a new cosine term $\cos(4\phi_i - 4\phi_j)$ ($\epsilon\epsilon' = +1$). Having $2 - 8K$ as its scaling dimension at $T = 0$, the

new cosine term is irrelevant around $K \simeq 1$ and we omit this. The second case with $\epsilon\epsilon' = -1$ can be further calculated as

$$\begin{aligned}
 (i = m, j = n, \epsilon\epsilon' = -1) &= \frac{1}{8} \int d^2\mathbf{r} \int d^2\mathbf{r}' \sum_{i,j}^{i \neq j} J_{i-j} J_{i-j} \sum_{\epsilon=\pm 1} e^{i\epsilon 2[\phi_i^<(\mathbf{r}) - \phi_j^<(\mathbf{r}) - \phi_i^<(\mathbf{r}') + \phi_j^<(\mathbf{r}')] } \\
 &\quad \langle e^{i\epsilon 2[\phi_i^>(\mathbf{r}) - \phi_j^>(\mathbf{r}) - \phi_i^>(\mathbf{r}') + \phi_j^>(\mathbf{r}')] } \rangle_{>} \left(1 - e^{-8\langle \phi_i^>(\mathbf{r}) \phi_i^>(\mathbf{r}') \rangle_{>}} \right) \\
 &= \frac{1}{4} \int d^2\mathbf{r} \int d^2\mathbf{r}' \sum_{i,j} J_{i-j} J_{i-j} : \cos(2[\phi_i^<(\mathbf{r}) - \phi_j^<(\mathbf{r}) - \phi_i^<(\mathbf{r}') + \phi_j^<(\mathbf{r}')]) : \\
 &\quad e^{-4KF_{1,\Lambda}(\mathbf{r}-\mathbf{r}')} 8dlKM_{\Lambda}(\mathbf{r}-\mathbf{r}') + \mathcal{O}(dl^2). \tag{B19}
 \end{aligned}$$

As above, we employ the gradient expansion and keep the leading order. This leads to the two-loop correction to the Luttinger parameter;

$$\begin{aligned}
 (i = m, j = n, \epsilon\epsilon' = -1) &= 2 \int d^2\mathbf{r} \sum_{i,j} J_{i-j}^2 \\
 &: \sum_{\mu=z,\tau} [\partial_{\mu}\phi_i^<(\mathbf{r}) - \partial_{\mu}\phi_j^<(\mathbf{r}')]^2 : D(\Lambda)K dl + \dots,
 \end{aligned}$$

with

$$D(\Lambda) \equiv \int d^2\mathbf{r} r^2 e^{-4KF_{1,\Lambda}(\mathbf{r})} M_{\Lambda}(\mathbf{r}).$$

Since $J_{i-j} = \frac{\tilde{g}}{L_x} \frac{1}{\pi\sqrt{2\pi}l'} e^{-\frac{(y_i - y_j)^2}{2l'^2}}$ (see Eq. (A19)), the summation over integer j results in a correction which is at most on the order of $1/L_x$. In the leading order in $1/L_x$, we thus can ignore this correction.

Half electron filling case

The partition function Eq. (B2) is expanded in the interchain rigidity term and umklapp term up to the second order;

$$\begin{aligned}
 \frac{Z}{Z_0} &= \frac{1}{Z_0^<} \sum_{\{\sigma_j^z\}} \int d\phi^< \exp \left[-S_0(\phi^<) + \dots + \frac{1}{2} \int d^2\mathbf{r} \sum_{\epsilon=\pm} \sum_{i,j} U_{i-j} \sigma_i^z \sigma_j^z e^{i\epsilon 2[\phi_i^<(\mathbf{r}) + \phi_j^<(\mathbf{r})]} \langle e^{i\epsilon 2[\phi_i^>(\mathbf{r}) + \phi_j^>(\mathbf{r}')] } \rangle_{>} \right. \\
 &\quad + \frac{1}{8} \int d^2\mathbf{r} \int d^2\mathbf{r}' \sum_{\epsilon,\epsilon'=\pm} \sum_{i,j}^{i \neq j} \sum_{m,n}^{m \neq n} U_{i-j} U_{m-n} \sigma_i^z \sigma_j^z \sigma_m^z \sigma_n^z e^{i\epsilon 2[\phi_i^<(\mathbf{r}) + \phi_j^<(\mathbf{r}')] } e^{i\epsilon' 2[\phi_m^<(\mathbf{r}') + \phi_n^<(\mathbf{r}')] } \\
 &\quad \left(\langle e^{i\epsilon 2[\phi_i^>(\mathbf{r}) + \phi_j^>(\mathbf{r}')] } \rangle_{>} e^{i\epsilon' 2[\phi_m^>(\mathbf{r}') + \phi_n^>(\mathbf{r}')] } \rangle_{>} - \langle e^{i\epsilon 2[\phi_i^>(\mathbf{r}) + \phi_j^>(\mathbf{r}')] } \rangle_{>} \langle e^{i\epsilon' 2[\phi_m^>(\mathbf{r}') + \phi_n^>(\mathbf{r}')] } \rangle_{>} \right) \\
 &\quad + \frac{1}{4} \int d^2\mathbf{r} \int d^2\mathbf{r}' \sum_{\epsilon,\epsilon'=\pm} \sum_{i,j}^{i \neq j} \sum_{m,n}^{m \neq n} J_{i-j} U_{m-n} \sigma_i^z \sigma_j^z \sigma_m^z \sigma_n^z e^{i\epsilon 2[\phi_i^<(\mathbf{r}) - \phi_j^<(\mathbf{r}')] } e^{i\epsilon' 2[\phi_m^<(\mathbf{r}') + \phi_n^<(\mathbf{r}')] } \\
 &\quad \left. \left(\langle e^{i\epsilon 2[\phi_i^>(\mathbf{r}) - \phi_j^>(\mathbf{r}')] } \rangle_{>} e^{i\epsilon' 2[\phi_m^>(\mathbf{r}') + \phi_n^>(\mathbf{r}')] } \rangle_{>} - \langle e^{i\epsilon 2[\phi_i^>(\mathbf{r}) - \phi_j^>(\mathbf{r}')] } \rangle_{>} \langle e^{i\epsilon' 2[\phi_m^>(\mathbf{r}') + \phi_n^>(\mathbf{r}')] } \rangle_{>} \right) \right] + \mathcal{O}(J^3, U^3, J^2U, JU^2) \tag{B20}
 \end{aligned}$$

where \dots are same as in Eq. (B8). As in the previous section, the first term (other than “ $-S_0[\phi^<] + \dots$ ”) within the exponent gives a one-loop RG correction to the umklapp term. The second term with $i = m, j \neq n$

and $\epsilon\epsilon' = -1$ give a two-loop correction to the interchain rigidity term. The last term with $i = m, j \neq n$ and $\epsilon\epsilon' = -1$ gives a two-loop correction to the umklapp term. Other cases generate irrelevant cosine terms or

can be omitted up to the leading order in $1/L_x$. Together with Eq. (B18), we finally obtain the RG equations for J_{j-m} , U_{j-m} and temperature T as in Eqs. (B5,B6).

RG phase diagram

Eqs. (B5,B6) are functional RG equations for J_m and U_m for all m . To gain simple ideas of these functional RG equations, we reduce them into RG equations for the following two coupling constants,

$$J \equiv \sum_m J_m, \quad U \equiv \sum_m U_m. \quad (\text{B21})$$

By taking the summation over the integer j in Eqs. (B5,B6), we obtain the RG equations for these two coupling constants;

$$\frac{dJ}{dl} = \left[2 - 2K \coth \frac{\Lambda}{2T} \right] J + KC[J^2 + U^2], \quad (\text{B22})$$

$$\frac{dU}{dl} = \left[2 - 2K \coth \frac{\Lambda}{2T} \right] U + 2KCJU, \quad (\text{B23})$$

with $dT/dl = T$.

Without the umklapp term ($U = 0$), three distinct fixed points are identified at $T = 0$ phase diagram; (i) $J = 0$ (decoupled one-dimensional chains: normal-phase fixed point) (ii) $J = +\infty$ (the displacement field shows a long-range order, $\langle \phi_j(z) \rangle = \phi_0$; DW-phase fixed point) (iii) $J = -J_0 < 0$ (a ‘frustrated’ fixed point). We call the fixed point with negative J to be ‘frustrated’ fixed point, because there are no obvious classical solutions of $\phi_j(z)$ which minimize the interchain interaction term with negative J ; for negative J , the extensive number of chains are antiferromagnetically coupled with one another within the magnetic length l . At $T = 0$, the Luttinger parameter has a critical value $K = K_c$ above which infinitesimal small J is always irrelevant, and below which small positive/negative J goes to the DW fixed point/‘frustrated’ fixed point respectively. At finite temperature, the critical value K_c goes to zero (Fig. 11(b)). There is a finite-temperature phase transition between the DW phase with a fixed point of $J = +\infty$ and $T \neq 0$ and the normal phase with a fixed point of $J = 0$ and $T = +\infty$ (Figs. 11(c,d)).

RG phase diagrams with the umklapp term are determined by three fixed points, (i) $(J, U) = (0, 0)$ normal phase fixed point, (ii) $(J, U) = (+\infty, +\infty)$ DW-phase fixed point and (iii) $(J, U) = (-|J_0|, 0)$ frustrated fixed point. As shown in Figs. 12(a,b), the interchain rigidity and the umklapp term help with each other for positive J , so that they grow up into the DW-phase fixed point. For negative J , the umklapp term is always renormalized to zero, which leads to either the normal phase fixed point ($K > K_c$) or the frustrated fixed point ($K < K_c$).

Appendix C: conductivity calculation

1. Imaginary-time time-ordered correlation function and its path integral

In terms of respective Lehmann representation, the real-time correlation function in eq. (31) is obtained from an imaginary-time time-ordered function by an analytic continuation in the complex ω plane,

$$\sigma_{zz}(\omega) = Q_{zz}(i\omega_n = \omega + i\eta), \quad (\text{C1})$$

$$Q_{zz}(i\omega_n) \equiv \int_0^\beta d\tau Q_{zz}(\tau) e^{i\omega_n \tau}, \quad (\text{C2})$$

$$Q_{zz}(\tau) \equiv -\frac{1}{V} \text{Tr}[\hat{\rho}_G T_\tau \{ \hat{J}_z(\tau) \hat{P}_z \}], \quad (\text{C3})$$

with $\hat{J}_z(\tau) \equiv e^{\hat{K}\tau} \hat{J}_z e^{-\hat{K}\tau}$. \hat{J}_z and \hat{P}_z are given by

$$\hat{J}_z = \frac{|e|uK}{\pi} \sum_j \int dz \partial_z \hat{\theta}_j(z),$$

$$\hat{P}_z = -\frac{|e|}{\pi} \sum_j \int dz \hat{\chi}_j(z).$$

$\hat{\rho}_G$ and \hat{K} are given by eqs. (38,39).

The imaginary-time correlation function $Q_{zz}(\tau)$ can be further calculated by a path integral, where the quantum statistical ensemble average with respect to Eqs. (38,39) can be carried out by a Gaussian integral over complex variables $\chi_j(z, \tau)$ and $\theta_j(z, \tau)$,

$$Q_{zz}(\tau) = \frac{e^2 u K}{\pi^2 V} \sum_{j,m} \int dz \int dz' R_{jm}(\tau; z, z'), \quad (\text{C4})$$

$$R_{jm}(\tau; z, z') \equiv \frac{\int \mathcal{D}\chi \mathcal{D}\theta e^{-S} \partial_z \theta_j(z, \tau) \chi_m(z', 0)}{\int \mathcal{D}\chi \mathcal{D}\theta e^{-S}}.$$

Here the action S is given by

$$\begin{aligned} -S = & -\frac{1}{2\beta L_z N} \sum_{\mathbf{K}} (\theta^*(\mathbf{K}) \chi^*(\mathbf{K})) [M_0(\mathbf{K})] \begin{pmatrix} \theta(\mathbf{K}) \\ \chi(\mathbf{K}) \end{pmatrix} \\ & -\frac{1}{L_z N} \sum_{\mathbf{k}} X(-\mathbf{k}) \chi(\mathbf{k}, i\omega_n = 0) \\ & -\frac{1}{\beta(L_z N)^2} \sum_{i\omega_n, \mathbf{k}, \mathbf{k}'} Y(-\mathbf{k}') \chi^*(\mathbf{k} - \mathbf{k}', i\omega_n) \chi(\mathbf{k}, i\omega_n), \end{aligned} \quad (\text{C5})$$

with a 2×2 matrix

$$[M_0(\mathbf{K})] \equiv \begin{pmatrix} \frac{uKk_z^2}{\pi} & \frac{ik_z \omega_n}{\pi} \\ \frac{ik_z \omega_n}{\pi} & \frac{uk_z^2}{\pi K} + 2J(k) + 2U(k) \end{pmatrix}, \quad (\text{C6})$$

and

$$\begin{aligned} J(k) & \equiv \sum_{n=1}^N J_n |1 - e^{iky_n}|^2, \\ U(k) & \equiv \sum_{n=1}^N U_n |1 + e^{iky_n}|^2. \end{aligned} \quad (\text{C7})$$

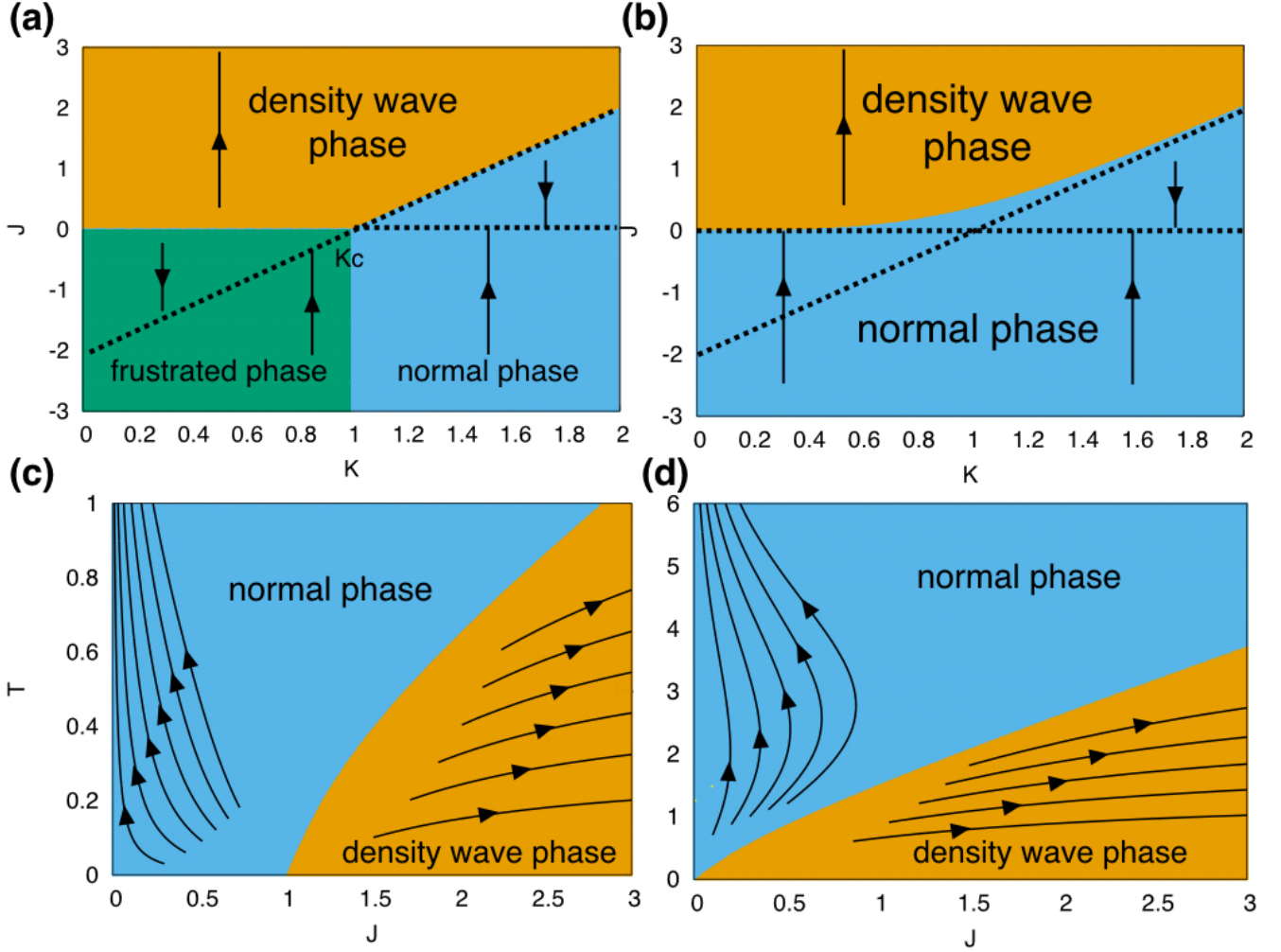


FIG. 11. RG phase diagrams at incommensurate electron filling case (i) normal phase (blue), (ii) DW phase (orange), and (iii) “frustrated” phase (green). The RG fixed lines (black dashed line), and RG trajectory (black solid line with arrow) are shown. (a) $T = 0$ $K - J$ phase diagram; (b) Finite temperature ($T=0.01$) $K - J$ phase diagram. (c) $T - J$ phase diagram for $K = 1.5$; (d) $T - J$ phase diagram for $K = 0.5$.

In eq. (C5), we used

is given by

$$\begin{aligned}
 (\chi_j(z, \tau), \theta_j(z, \tau)) &\equiv \frac{1}{\beta L_z N} \sum_{\mathbf{K}} e^{-i\omega_n \tau + i k_z z + i k_y y_j} \\
 &\quad \times (\chi(\mathbf{k}, i\omega_n), \theta(\mathbf{k}, i\omega_n)), \\
 (X_j(z), Y_j(z)) &\equiv \frac{1}{L_z N} \sum_{\mathbf{k}} e^{i k_z z + i k_y y_j} (X(\mathbf{k}), Y(\mathbf{k})),
 \end{aligned}$$

with $N \equiv L_x L_y / (2\pi l^2)$, the magnetic length l , $\mathbf{K} \equiv (\mathbf{k}, i\omega_n) \equiv (k_z, k, i\omega_n)$, $\mathbf{K}' \equiv (\mathbf{k}', i\omega'_n) \equiv (k'_z, k', i\omega'_n)$. k_z and k are wave vectors conjugate to z and y_j (chain index) respectively. $i\omega_n$ is bosonic Matsubara frequency $i\omega_n = 2n\pi/\beta$. In the \mathbf{K} space, the correlation function

$$\begin{aligned}
 R_{j,m}(\tau; z, z') &\equiv \frac{1}{(\beta L_z N)^2} \sum_{\mathbf{K}, \mathbf{K}'} e^{i\omega_n \tau - i k_z z - i k_y y_j} e^{i k'_z z' + i k' y_m} \\
 &\quad \times (-i k_z) \frac{\int \mathcal{D}\chi \mathcal{D}\theta \theta^*(\mathbf{k}, i\omega_n) \chi(\mathbf{k}', i\omega'_n) e^{-S}}{\int \mathcal{D}\chi \mathcal{D}\theta e^{-S}}. \quad (C8)
 \end{aligned}$$

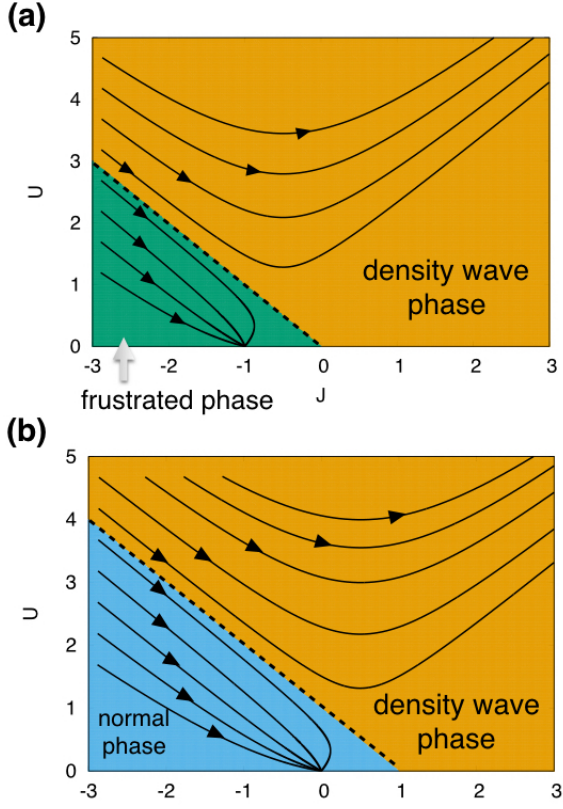


FIG. 12. $T = 0$ $J - U$ phase diagrams at half electron filling case. (i) normal phase (blue), (ii) CDW phase (orange), and (iii) “frustrated” phase (green). (a) $J - U$ phase diagram at $K = 0.5$; (b) $J - U$ phase diagram at $K = 1.5$.

2. Generating function formulation

The integrand in Eq. (C8) can be generated from a partition function in the presence of external fields,

$$\begin{aligned} & \frac{\int \mathcal{D}\chi \mathcal{D}\theta \theta^*(\mathbf{k}, i\omega_n) \chi(\mathbf{k}', i\omega'_n) e^{-S}}{\int \mathcal{D}\chi \mathcal{D}\theta e^{-S}} \\ &= \left(\frac{\partial^2 \ln Z[A, B]}{\partial B(\mathbf{K}) \partial A^*(\mathbf{K}')} \right)_{|A, B \equiv 0} \\ &+ \left(\frac{\partial \ln Z[A, B]}{\partial B(\mathbf{K})} \right)_{|A, B \equiv 0} \left(\frac{\partial \ln Z[A, B]}{\partial A^*(\mathbf{K}')} \right)_{|A, B \equiv 0}, \quad (\text{C9}) \end{aligned}$$

where the partition function is given by

$$\begin{aligned} Z[A, B] &\equiv \int \mathcal{D}\chi \mathcal{D}\theta e^{-S[A, B]}, \\ -S[A, B] &\equiv -S + \sum_{\mathbf{K}} \left[\begin{pmatrix} B^*(\mathbf{K}) & A^*(\mathbf{K}) \end{pmatrix} \begin{pmatrix} \theta(\mathbf{K}) \\ \chi(\mathbf{K}) \end{pmatrix} \right. \\ &\quad \left. + \begin{pmatrix} \theta^*(\mathbf{K}) & \chi^*(\mathbf{K}) \end{pmatrix} \begin{pmatrix} B(\mathbf{K}) \\ A(\mathbf{K}) \end{pmatrix} \right], \end{aligned}$$

with S in eq. (C5). A Gaussian integration over $\theta(\mathbf{K})$ and $\chi(\mathbf{K})$ leads to a free energy,

$$\begin{aligned} \ln Z[A, B] &= \ln Z[A = 0, B = 0] + \\ &\sum_{\alpha, \beta=1,2} \sum_{\mathbf{K}, \mathbf{K}'} \left(B^*(\mathbf{K}), A^*(\mathbf{K}) - \mathbf{X}^*(\mathbf{K}) \right)_{\alpha} \\ &\quad \times [M^{-1}]_{(\alpha, \mathbf{K} | \beta, \mathbf{K}')} \left(\begin{pmatrix} B(\mathbf{K}') \\ A(\mathbf{K}') - \mathbf{X}(\mathbf{K}') \end{pmatrix} \right)_{\beta}, \quad (\text{C10}) \end{aligned}$$

with

$$\mathbf{X}(\mathbf{K}) \equiv \frac{1}{2L_z N} \mathbf{X}(\mathbf{k}) \delta_{\omega_n, 0}, \quad (\text{C11})$$

and

$$\begin{aligned} [M]_{(\alpha, \mathbf{K} | \beta, \mathbf{K}')} &\equiv \frac{1}{2\beta L_z N} [M_0(\mathbf{K})]_{\alpha, \beta} \delta_{\mathbf{K}, \mathbf{K}'} \\ &+ \frac{1}{\beta (L_z N)^2} Y(\mathbf{k} - \mathbf{k}') \delta_{\omega_n, \omega'_n} \delta_{\alpha, 2} \delta_{2, \beta}, \\ [M^{-1}]_{(\alpha, \mathbf{K} | \beta, \mathbf{K}')} &\equiv 2\beta L_z N \delta_{\omega_n, \omega'_n} \left\{ [M_0^{-1}(\mathbf{k}, \omega_n)]_{\alpha, \beta} \delta_{\mathbf{k}, \mathbf{k}'} \right. \\ &- \frac{2}{L_z N} [M_0^{-1}(\mathbf{k}, \omega_n)]_{\alpha, 2} [M_0^{-1}(\mathbf{k}', \omega_n)]_{2, \beta} Y(\mathbf{k} - \mathbf{k}') + \\ &\sum_{m=2}^{\infty} \frac{(-1)^m 2^m}{(L_z N)^m} \sum_{\mathbf{k}_3, \dots, \mathbf{k}_{m+1}} [M_0^{-1}(\mathbf{k}, \omega_n)]_{\alpha, 2} [M_0^{-1}(\mathbf{k}_1, \omega_n)]_{2, 2} \\ &\quad \dots [M_0^{-1}(\mathbf{k}_{m-1}, \omega_n)]_{2, 2} [M_0^{-1}(\mathbf{k}', \omega_n)]_{2, \beta} \times \\ &\quad \left. \times Y(\mathbf{k} - \mathbf{k}_1) \dots Y(\mathbf{k}_{m-2} - \mathbf{k}_{m-1}) Y(\mathbf{k}_{m-1} - \mathbf{k}') \right\}. \quad (\text{C12}) \end{aligned}$$

The Y -field does not carry frequency and couples only between two χ -fields. Thus, $[M^{-1}]_{(2, \mathbf{K} | 1, \mathbf{K}')}$ is always proportional to $[M_0^{-1}(\mathbf{k}', i\omega_n)]_{2, 1}$. Since $[M_0^{-1}(\mathbf{k}', i\omega_n)]_{2, 1}$ vanishes at $i\omega_n = 0$ and $\mathbf{X}(\mathbf{K})$ vanishes at $i\omega_n \neq 0$ (see eq. (C6, C11) respectively), the 2nd term in the right hand side of eq. (C9) does not contribute;

$$\frac{\int \mathcal{D}\chi \mathcal{D}\theta \theta^*(\mathbf{k}, i\omega_n) \chi(\mathbf{k}', i\omega'_n) e^{-S}}{\int \mathcal{D}\chi \mathcal{D}\theta e^{-S}} = [M^{-1}]_{(2, \mathbf{K}' | 1, \mathbf{K})}. \quad (\text{C13})$$

3. Quenched disorder average and Born approximation

The conductivity in a given disorder realization was calculated so far. In the following, the conductivity will be further averaged over different disorder realizations. For simplicity, we take this average by

$$\begin{aligned} \overline{\dots} &= \\ &\frac{\int \mathcal{D}X_j(z) \mathcal{D}Y_j(z) \dots e^{-\frac{1}{g_x} \sum_j \int dz X_j^2(z) - \frac{1}{g_y} \sum_j \int dz Y_j^2(z)}}{\int \mathcal{D}X_j(z) \mathcal{D}Y_j(z) e^{-\frac{1}{g_x} \sum_j \int dz X_j^2(z) - \frac{1}{g_y} \sum_j \int dz Y_j^2(z)}}. \quad (\text{C14}) \end{aligned}$$

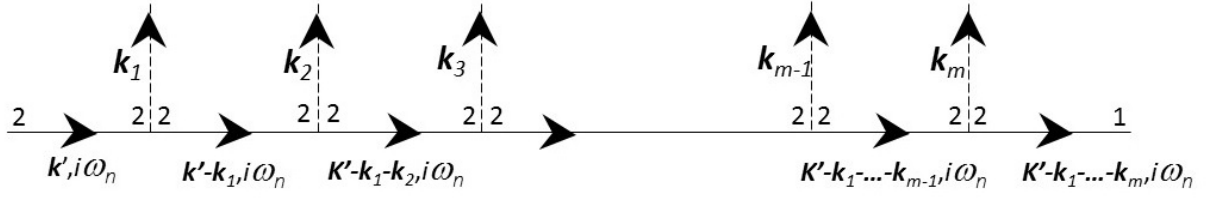


FIG. 13. (color online) Feynman diagram for the conductivity along the field direction. Solid line with arrow represents the phason fields; χ field denoted by “2” and θ field denoted by “1”. Dotted line with arrow represents the impurity fields (Y-field).

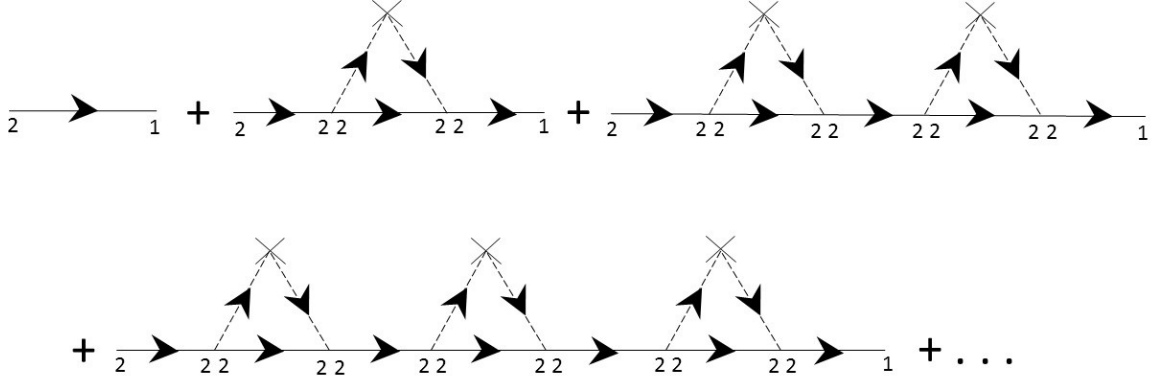


FIG. 14. (color online) Feynman diagrams for Born approximation, in which the self-energy is evaluated in the lowest order approximation.

To this end, we have only to take the disorder average of $[M^{-1}]_{(2, \mathbf{K}'|1, \mathbf{K})}$ given in eq. (C12). The average leads to a pair contraction among even integer number of the Y-fields in Eq. (C12), such that a pair of two impurity lines (Y-field lines) contracted share a same momentum,

Eqs. (C4, C8, C13, C12, C15) lead to

$$\overline{Y(\mathbf{k}_1)Y(\mathbf{k}_2)\cdots Y(\mathbf{k}_{2M})} = \left(\frac{g_y L_z N}{2}\right)^M \times \sum_{\sigma} \delta_{\mathbf{k}_{\sigma(1)} + \mathbf{k}_{\sigma(2)}, 0} \delta_{\mathbf{k}_{\sigma(3)} + \mathbf{k}_{\sigma(4)}, 0} \cdots \delta_{\mathbf{k}_{\sigma(2M-1)} + \mathbf{k}_{\sigma(2M)}, 0}. \quad (\text{C15})$$

Here the summation over σ denotes a sum of all possible permutation among $2M$ impurity lines under the following conditions: $\sigma(2j-1) < \sigma(2j)$ ($j = 1, 2, \dots, M$) and $\sigma(1) < \sigma(3) < \cdots < \sigma(2M-1)$. Those terms with odd integer number impurity lines vanish under the average. The momentum conservation at every impurity vertex makes the two external momenta in Eq.(C12) to be same, $\mathbf{k} = \mathbf{k}'$.

$$\begin{aligned} \overline{Q_{zz}(\tau)} &= \frac{2e^2 u K}{\pi^2 V} \sum_{j,m} \int dz \int dz' \frac{1}{\beta L_z N} \sum_{\omega_n, \mathbf{k}} e^{i\omega_n \tau} \\ &\quad e^{-ik_z(z-z') - ik_x(y_j - y_m)} (-ik_z) \left\{ 1 + \sum_{M=1}^{\infty} \frac{(2g_y)^M}{(L_z N)^M} \times \right. \\ &\quad \sum_{\sigma} \sum_{\mathbf{k}_1, \mathbf{k}_2, \dots, \mathbf{k}_{2M}} \delta_{\mathbf{k}_{\sigma(1)} + \mathbf{k}_{\sigma(2)}, 0} \cdots \delta_{\mathbf{k}_{\sigma(2M-1)} + \mathbf{k}_{\sigma(2M)}, 0} \times \\ &\quad [M_0^{-1}(\mathbf{k}, \omega_n)]_{2,2} [M_0^{-1}(\mathbf{k} - \mathbf{k}_1, \omega_n)]_{2,2} \cdots \\ &\quad \left. [M_0^{-1}(\mathbf{k} - \mathbf{k}_1 \cdots - \mathbf{k}_{2M-1}, \omega_n)]_{2,2} \right\} [M_0^{-1}(\mathbf{k}, \omega_n)]_{2,1}. \end{aligned} \quad (\text{C16})$$

With Eq. (C2), we may rewrite this as,

$$\begin{aligned}
\overline{Q_{zz}(i\omega_n)} &= \frac{2e^2 u K}{\pi^2 V} \sum_{k_z, k, l} \int dz'' e^{-ik_z z'' - ik_y l} \\
&\frac{\pi \omega_n}{u^2 k_z^2 + 2u\pi K [J(k) + U(k)] + \omega_n^2} \left\{ 1 + \sum_{M=1}^{\infty} \frac{(2g_y)^M}{(L_z N)^M} \right. \\
&\sum_{\sigma} \sum_{\mathbf{k}_1, \mathbf{k}_2, \dots, \mathbf{k}_{2M}} \delta_{\mathbf{k}_{\sigma(1)} + \mathbf{k}_{\sigma(2)}, 0} \cdots \delta_{\mathbf{k}_{\sigma(2M-1)} + \mathbf{k}_{\sigma(2M)}, 0} \times \\
&[M_0^{-1}(\mathbf{k}, \omega_n)]_{2,2} [M_0^{-1}(\mathbf{k} - \mathbf{k}_1, \omega_n)]_{2,2} \cdots \\
&\cdots [M_0^{-1}(\mathbf{k} - \mathbf{k}_1 \cdots - \mathbf{k}_{2M-1}, \omega_n)]_{2,2} \left. \right\} \\
&= \frac{e^2 u K}{\pi^2 l^2} \frac{\omega_n}{2u\pi K U(0) + \omega_n^2} \left\{ 1 + \sum_{M=1}^{\infty} \frac{(2g_y)^M}{(L_z N)^M} \right. \\
&\sum_{\sigma} \sum_{\mathbf{k}_1, \mathbf{k}_2, \dots, \mathbf{k}_{2M}} \delta_{\mathbf{k}_{\sigma(1)} + \mathbf{k}_{\sigma(2)}, 0} \cdots \delta_{\mathbf{k}_{\sigma(2M-1)} + \mathbf{k}_{\sigma(2M)}, 0} \times \\
&[M_0^{-1}(\mathbf{k} = 0, \omega_n)]_{2,2} [M_0^{-1}(-\mathbf{k}_1, \omega_n)]_{2,2} \cdots \\
&\cdots [M_0^{-1}(-\mathbf{k}_1 \cdots - \mathbf{k}_{2M-1}, \omega_n)]_{2,2} \left. \right\}, \quad (\text{C17})
\end{aligned}$$

with $J(0) = 0$. From eq. (C16) to eq. (C17), we took the integral over the center-of-mass coordinates, $Z \equiv \frac{z+z'}{2}$ and $n \equiv \frac{j+m}{2}$;

$$\int dz \int dz' = \int dZ \int dz'' = L_z \int dz'', \sum_{j,m} = N \sum_l,$$

with $z'' \equiv z - z'$ and $l \equiv j - m$. From the first line to the second line in eq. (C17), we took the integral over the relative coordinates z'' and l , making the external momenta to be zero, $k_z = k = 0$.

Generally, it is hard to carry out analytically the summation over all possible permutations in Eq.(C17). To gain a simple idea, we employ the lowest order approximation for a self-energy (Born approximation; compare Fig. 13 with Fig. 14). This leads to

$$\begin{aligned}
\overline{Q_{zz}(i\omega_n)} &= \frac{e^2 u K}{\pi^2 l^2} \frac{\omega_n}{2u\pi K U(0) + \omega_n^2} \\
&\times \sum_{M=0}^{\infty} \left(\frac{2g_y}{L_z N} [M_0^{-1}(0, \omega_n)]_{2,2} \sum_{\mathbf{k}} [M_0^{-1}(\mathbf{k}, \omega_n)]_{2,2} \right)^M \\
&= \frac{e^2 u K}{\pi^2 l^2} \frac{\omega_n}{\omega_n^2 + 2u\pi K U(0) - \frac{2\pi u K g_y}{L_z N} \sum_{\mathbf{k}} [M_0^{-1}(\mathbf{k}, \omega_n)]_{2,2}}, \quad (\text{C18})
\end{aligned}$$

with

$$[M_0^{-1}(\mathbf{k}, \omega_n)]_{2,2} = \frac{\pi u K}{E^2(k_z, k) + \omega_n^2}, \quad (\text{C19})$$

$$E(k_z, k) = \sqrt{u^2 k_z^2 + 2u\pi K (J(k) + U(k))}. \quad (\text{C20})$$

Eqs. (C18,C19,C20) are nothing but eqs. (42,43,44) respectively.

4. chemical potential type disorder case

We can also carry out the same calculation of the conductivity with a chemical potential type disorder,

$$H_{\text{imp}}^{\text{chem}} = \sum_j \int dz \rho_j(z) \partial_z \chi_j(z). \quad (\text{C21})$$

Following the same process up to Eq. (C13), the Fourier transformed Matsubara Green function is given by,

$$\begin{aligned}
&\frac{\int \mathcal{D}\chi \mathcal{D}\theta \theta^*(\mathbf{k}, i\omega_n) \chi(\mathbf{k}', i\omega'_n) e^{-S}}{\int \mathcal{D}\chi \mathcal{D}\theta e^{-S}} = [M_0^{-1}]_{(2, \mathbf{K}|1, \mathbf{K})} \delta_{\mathbf{K}, \mathbf{K}'} \\
&+ \sum_{\mathbf{K}_1, \mathbf{K}_2} [M_0^{-1}]_{(2, \mathbf{K}'|2, \mathbf{K}_2)} \mathbf{W}(\mathbf{K}_2) \mathbf{W}^*(\mathbf{K}_1) [M_0^{-1}]_{(2, \mathbf{K}_1|1, \mathbf{K})} \quad (\text{C22})
\end{aligned}$$

with the impurity field $\mathbf{W}(\mathbf{K}) \equiv -\frac{1}{2L_z N} (ik_z) \rho(\mathbf{k}) \delta_{\omega_n, 0}$. Due to the same reason given above Eq. (C13), the second term vanishes in eq. (C22). Thus, we see that the chemical potential type disorder has no influence on the (optical) conductivity.

Appendix D: single-particle spectral function calculation

The four-point correlation function in the frozen lattice superconductor (FLS) model is calculated in the two limiting cases; one is in the non-superconducting (SC) phase ('Maxwell phase') and the other is in the superconducting (SC) phase ('Meissner phase'). We evaluate the correlation function by respective free theories. By use of eq. (73), we obtain a Fourier transform of the single-particle Matsubara Green function, and, by an analytic continuation, we obtain a single-particle spectral function. The next subsection begins with the four-point correlation function in the SC phase of the FLS model, which gives the spectral function in the normal phase in the XY model. The next next subsection begins with the correlation function in the non-SC phase of FLS model, which gives the spectral function in the DW phase in the XY model.

1. Meissner phase in the FLS model (normal phase in the XY model)

In the Meissner phase, the U(1) phase of the SC order parameter exhibits a long range order and the gauge field is expelled from the SC bulk. Thus, we omit the coupling between gauge field and U(1) phase, and expand the cosine term with respect to a gradient of the U(1) phase;

$$S_{\text{FLS}}[\mathbf{a}_{\vec{j}}, \theta_{\vec{j}}] \simeq -\frac{1}{2t} \sum_{\vec{j}, \mu} (\Delta_{\mu} \theta_{\vec{j}})^2. \quad (\text{D1})$$

With this Gaussian theory, the four-points correlation function is evaluated,

$$\begin{aligned} & \langle e^{i\theta\mathbf{N}_1 - i\theta\mathbf{N}_1 + a_y e_y - i\theta\mathbf{N}_2 + i\theta\mathbf{N}_2 + a_y e_y} \rangle \\ & \equiv \exp \left[-C + t f(z_1 - z_2, \tau_1 - \tau_2) \right], \end{aligned} \quad (\text{D2})$$

with Eq. (65). The constant C in eq. (D2) is given by

$$C = \frac{t}{\beta L_z L_y} \sum_{k_z, k_y, \omega_n} \frac{|1 - e^{ik_y a_y}|^2}{6 - 2 \cos k_y a_y - 2 \cos k_z a_z - 2 \cos \omega_n a_\tau}.$$

$f(z, \tau)$ and its Fourier component is calculated as

$$\begin{aligned} f(z, \tau) & \equiv \frac{1}{\beta L_z} \sum_{\omega_n, q_z} e^{iq_z z - i\omega_n \tau} \mathcal{F}(q_z, i\omega_n) \\ \mathcal{F}(q_z, i\omega_n) & = \frac{1}{L_y} \sum_{q_y} \frac{2 - 2 \cos q_y a_y}{6 - 2 \cos q_y a_y - 2 \cos q_z a_z - 2 \cos \omega_n a_\tau} \\ & = 1 - \sqrt{\frac{4 - 2 \cos q_z a_z - 2 \cos \omega_n a_\tau}{8 - 2 \cos q_z a_z - 2 \cos \omega_n a_\tau}} \\ & = 1 - \frac{\sqrt{q_z^2 + \omega_n^2}}{2} + \dots, \end{aligned} \quad (\text{D3})$$

with bosonic Matsubara frequency, $i\omega_n = 2n\pi/\beta$. In the final line of eq. (D3), we took $u = 1$ and the lattice constants a_z, a_τ to be unit for simplicity.

Regarding t to be small, we further expand Eq. (D2) in t . The expansion together with Eq. (73) leads to the following expression of the Matsubara Green function,

$$\mathcal{G}_{\sigma,j}(z, \tau) = -e^{-C} \text{sgn}(\tau) \left\{ 1 + t f(z, \tau) + \mathcal{O}(t^2) \right\} \quad (\text{D4})$$

whose Fourier-transform is given by a convolution of the Fourier transform of the sign function and that of $f(z, \tau)$,

$$\begin{aligned} \mathcal{G}_{\sigma,j}(q_z, i\mathcal{E}_n) & \equiv \int_{-\infty}^{\infty} dz \frac{1}{2} \int_{-\beta}^{\beta} d\tau e^{-iq_z z + i\mathcal{E}_n \tau} \mathcal{G}_{\sigma,j}(z, \tau), \\ & = 2e^{-C} \delta(q_z) \frac{1}{i\mathcal{E}_n} \\ & \quad - \frac{te^{-C}}{\beta} \sum_{\mathcal{E}'_n} \frac{1}{i\mathcal{E}'_n} \sqrt{q_z^2 + (\mathcal{E}_n - \mathcal{E}'_n)^2} + \dots + \mathcal{O}(t^2). \end{aligned} \quad (\text{D5})$$

Here we used

$$\frac{1}{2} \int_{-\beta}^{\beta} \text{sgn}(\tau) e^{i\mathcal{E}_n \tau} d\tau = -\frac{1}{i\mathcal{E}_n} (1 - \cos \mathcal{E}_n \beta) = -\frac{2}{i\mathcal{E}_n}, \quad (\text{D6})$$

with fermionic Matsubara frequency $i\mathcal{E}_n \equiv (2n+1)\pi/\beta$ and $i\mathcal{E}'_n \equiv (2n'+1)\pi/\beta$. The summation over the frequency in the right hand side of eq. (D5) can be carried out by an integral in the low-temperature limit

($\beta \rightarrow 0$). After the analytic continuation of $\mathcal{G}_{\sigma,j}(q_z, i\mathcal{E}_n)$ ($i\mathcal{E}_n \rightarrow \omega \pm i\eta$), we obtain the spectral function,

$$\begin{aligned} \rho_\sigma(q_z, \omega) & \equiv \frac{1}{i} \left\{ \mathcal{G}_{\sigma,j}(q_z, i\mathcal{E}_n = \omega - i\eta) \right. \\ & \quad \left. - \mathcal{G}_{\sigma,j}(q_z, i\mathcal{E}_n = \omega + i\eta) \right\}, \\ & = 4\pi e^{-C} \delta(q_z) \delta(\omega) \\ & \quad + 2\pi t e^{-C} \sqrt{\omega^2 - q_z^2} \Theta(|\omega| - |q_z|). \end{aligned} \quad (\text{D7})$$

With the Fermi velocity u recovered, we obtain eqs. (11,76). The imaginary part of the real-time time-ordered Green function is given by the spectral function,

$$\begin{aligned} \text{Im } G_\sigma(q_z, \omega) & \equiv -\pi \tanh\left(\frac{\beta\omega}{2}\right) \rho_\sigma(q_z, \omega) \\ & = -\pi t e^{-C} \tanh\left(\frac{\beta\omega}{2}\right) \sqrt{\omega^2 - u^2 q_z^2} \Theta(|\omega| - u|q_z|). \end{aligned} \quad (\text{D8})$$

By the above derivation, the usage of these expressions may be limited to low-energy and long wavelength region; $q_z \ll a_z^{-1}, \omega \ll u a_z^{-1}$.

2. Maxwell phase in the FLS model (DW phase in the XY model)

In the Maxwell phase, the superconducting order is destroyed by the gauge fluctuation, while the gradient of the U(1) phase is locked into the associated gauge field under the ‘frozen’ limit ($t \rightarrow 0$);

$$\begin{aligned} \mathcal{G}_{\sigma,j}(z_1 - z_2, \tau_1 - \tau_2) & = \\ & - \text{sgn}(\tau_1 - \tau_2) \langle e^{i\theta\mathbf{N}_1 - i\theta\mathbf{N}_1 + a_y e_y - i\theta\mathbf{N}_2 + i\theta\mathbf{N}_2 + a_y e_y} \rangle \\ & = -\text{sgn}(\tau_1 - \tau_2) \langle e^{i2\pi a_{\mathbf{N}_1, y} - i2\pi a_{\mathbf{N}_2, y}} \rangle_{\text{FLS}}. \end{aligned} \quad (\text{D9})$$

Eq. (D9) is evaluated with respect to the free theory for the non-superconducting phase of the FLS model;

$$S_{\text{FLS}}[\mathbf{a}_{\vec{j}}, \theta_{\vec{j}}] \simeq -\frac{1}{2J} \sum_{j, \mu} (\nabla \times \mathbf{a})_{j, \mu}^2. \quad (\text{D10})$$

According to this free Maxwell term, two vortex segments separated by R interact via the Coulombic force $1/R^{31}$; the Matsubara Green function is given by,

$$\begin{aligned} \mathcal{G}_{\sigma,j}(z_1 - z_2, \tau_1 - \tau_2) & = \\ & - \text{sgn}(\tau_1 - \tau_2) \frac{4\pi^2 J}{\sqrt{(z_1 - z_2)^2 + (\tau_1 - \tau_2)^2}}. \end{aligned} \quad (\text{D11})$$

The Fourier transform of $\mathcal{G}_{\sigma,j}(z, \tau)$ is given by the following convolution,

$$\mathcal{G}_{\sigma,j}(q_z, i\mathcal{E}_n) = \frac{1}{\beta} \sum_{\mathcal{E}'_n} \frac{1}{i\mathcal{E}'_n} \frac{8\pi^2 J}{\sqrt{q_z^2 + (\mathcal{E}'_n - \mathcal{E}_n)^2}} \quad (\text{D12})$$

with the Matsubara frequency, $\mathcal{E}_n = (2n+1)\pi/\beta$. The summation over the fermionic Matsubara frequency in

the right hand side of Eq. (D12) is carried out by an integral in the low temperature limit ($\beta \rightarrow 0$). After the analytic continuation of $\mathcal{G}_{\sigma,j}(q_z, i\mathcal{E}_n)$ in the complex plane, we obtain the spectral function and the imaginary part of the real-time time-ordered Green function as fol-

lows;

$$\begin{aligned}\rho_{\sigma}(q_z, \omega) &= \frac{16\pi^3 J}{\sqrt{\omega^2 - u^2 q_z^2}} \Theta(|\omega| - u|q_z|), \\ \text{Im } G_{\sigma}(q_z, \omega) &= -\tanh\left(\frac{\beta\omega}{2}\right) \frac{16\pi^3 J}{\sqrt{\omega^2 - u^2 q_z^2}} \Theta(|\omega| - u|q_z|),\end{aligned}\tag{D13}$$

(see eq. (10,77)).

* rshindou@pku.edu.cn

- ¹ B. I. Halperin, Japanese Journal of Applied Physics, **26**, 1913 (1987).
- ² V Celli and N. D. Mermin, Phys. Rev. **140**, A839 (1965).
- ³ S. A. Brazovskii, Zh. Eksp. Teor. Fiz. **62**, 820 (1972) [Sov. Phys. JETP, **35**, 433 (1972)]; Zh. Eksp. Teor. Fiz. **61**, 2401 (1971) [Sov. Phys. JETP, **34**, 1286 (1972)].
- ⁴ W. G. Kleppmann and R. J. Elliott J. Phys. C Solid State Phys. **8** 2729 (1975).
- ⁵ E. W. Fenton, Phys. Rev. **170**, 816 (1968).
- ⁶ S. Mase and T. Sakai, J. Phys. Soc. Japan, **31** 730 (1971).
- ⁷ N. B. Brandt and S. M. Chudinov, J. Low Temp. Phys. **81** 339 (1972).
- ⁸ H. Fukuyama, Solid State Communications, **26**, 783, (1978).
- ⁹ S. Tanuma, R. Inaba, A. Furukawa, O. Takahashi, Y. Iye and Y. Onuki, *Physics in High Magnetic Fields*, ed. S. Chikazumi and N. Miura (Springer, Berlin, 1981), p.316.
- ¹⁰ Y. Iye, P. M. Tedrow, G. Timp, M. Shayegan, M. S. Dresselhaus, G. Dresselhaus, A. Furukawa, and S. Tanuma, Phys. Rev. B **25** 5478 (1982).
- ¹¹ Y. Iye and G. Dresselhaus, Phys. Rev. Lett. **54**, 1182 (1985).
- ¹² H. Yaguchi and J. Singleton Phys. Rev. Lett. **81**, 5193 (1998).
- ¹³ S. Uji, J. S. Brooks and Y. Iye, Physica B **246-247**, 299 (1998).
- ¹⁴ Y. Kopelevich, B. Raquet, M. Goiran, W. Escoffier, R. R. Da Silva, J. C. Medina Pantoja, I. A. Lukyanchuk, A. Sinchenko and P. Monceau, Phys. Rev. Lett. **103**, 116802 (2009).
- ¹⁵ A. Kumar, J. Poumirol, W. Escoffier, M. Goiran, B. Raquet, and J. C. Pivin, J. Phys. Condens. Matter **22** 436004 (2010).
- ¹⁶ B. Fauque, D. LeBoeuf, B. Vignolle, M. Nardone, C. Proust, and K. Behnia, Phys. Rev. Lett **110**, 266601 (2013).
- ¹⁷ K. Akiba, A. Miyake, H. Yaguchi, A. Matsuo, K. Kindo, and M. Tokunaga, J. Phys. Soc. Jpn. **84**, 054709 (2015).
- ¹⁸ K. Behnia, L. Balicas and Y. Kopelevich, Science **317**, 1729 (2007).
- ¹⁹ A. Banerjee, B. Fauque, K. Izawa, A. Miyake, I. Sheikin, J. Flouquet, B. Lenoir, and K. Behnia, Phys. Rev. B **78**, 161103(R) (2008).
- ²⁰ L. Li J. G. Checkelsky, Y. S. Hor, C. Uher, A. F. Hebard, R. J. Cava, and N. P. Ong, Science **321**, 547 (2008).
- ²¹ C. Zhang, Z. Lin, C. Guo, S. Y. Xu, C. C. Lee, H. Lu, S. M. Huang, G. Chang, C. H. Hsu, H. Lin, L. Li, C. Zhang, T. Neupert, M. Z. Hasan, J. Wang, S. Jia, arXiv:1507.06301.
- ²² C. Zhang, B. Tong, Z. Yuan, Z. Lin, J. Wang, C. Y. Xi, Z. Wang, S. Jia, C. Zhang arXiv:1601.05895.
- ²³ D. Yoshioka and H. Fukuyama, J. Phys. Soc. Jpn. **50**, 725 (1981).
- ²⁴ Z. Tesanovic and B. I. Halperin, Phys. Rev. B **36**, 4888 (1987).
- ²⁵ A. H. MacDonald and Garnett W. Bryant, Phys. Rev. Lett. **58**, 515 (1987).
- ²⁶ A. A. Abrikosov, J. Low Temp. Phys. **10**, 3 (1973).
- ²⁷ V. M. Yakovenko, Phys. Rev. B **47**, 8851 (1993).
- ²⁸ Y. Takada and H. Goto, J. Phys. Condens. Matter **10**, 11315 (1998).
- ²⁹ J. Alicea, and L. Balents, Phys. Rev. B **79** 241101 (R) (2009).
- ³⁰ S. W. Tsai, D. L. Maslov, and L. I. Glazman, Phys. Rev. B **65**, 241102 (R) (2002).
- ³¹ M. E. Peskin, Ann. Phys. **113**, 122 (1978).
- ³² C. Dasgupta and B. I. Halperin, Phys. Rev. Lett. **47**, 1556 (1981).
- ³³ I. Herbut, *A modern approach to critical phenomena*, (Cambridge University Press, 2007).
- ³⁴ T. Giamarchi, *Quantum physics in one dimension*, (Clarendon Press, Oxford, 2003).
- ³⁵ B. I. Halperin, Phys. Rev. B. **25**, 2185 (1982).
- ³⁶ L. Balents, and M. P. A. Fisher Phys. Rev. Lett., **76**, 2782 (1998).
- ³⁷ H. Fukuyama, J. Phys. Soc. Jpn. **41**, 513 (1976).
- ³⁸ S. Datta, *Electronic Transport in Mesoscopic Systems*, (Cambridge University Press, 1995).
- ³⁹ Y. Imry and S. Ma, Phys. Rev. Lett **35**, 21 (1975).
- ⁴⁰ L. J. Sham and B. R. Patton, Phys. Rev. B **13**, 3151 (1976).
- ⁴¹ H. Fukuyama and P. A. Lee, Phys. Rev. B **17**, 535 (1978).
- ⁴² A. L. Fetter and J. D. Walecka, *Quantum Theory of Many-Particle Systems*, (Dover Publications, Inc. Mineola, New York, 2003).
- ⁴³ P. Nozieres, and F. Gallet, J. Phys. (Paris), **48**, 353 (1987).